General Disclaimer

One or more of the Following Statements may affect this Document

- This document has been reproduced from the best copy furnished by the organizational source. It is being released in the interest of making available as much information as possible.

- This document may contain data, which exceeds the sheet parameters. It was furnished in this condition by the organizational source and is the best copy available.

- This document may contain tone-on-tone or color graphs, charts and/or pictures, which have been reproduced in black and white.

- This document is paginated as submitted by the original source.

- Portions of this document are not fully legible due to the historical nature of some of the material. However, it is the best reproduction available from the original submission.

LASER SPACE RENDEZVOUS AND DOCKING SYSTEM STUDY CONTINUATION

Final Report for the Period
Febuary 1976 - June 1977

1257 R 0013

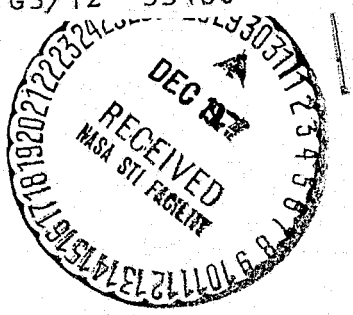

Written by:

S. Adelman
H. Heynau
S. Levinson
F. Weindling

Prepared for:

George C. Marshall Space Flight Center
Marshall Space Flight Center, Alabama
Contract No. NAS8-31489

Prepared by:

Norden Division of United Technologies Corp.
Norwalk, Connecticut

30 June 1977

ABSTRACT

Under Contract NAS8-31489 with the National Aeronautics and Space Administration/Marshall Space Flight Center (NASA/MSFC), Norden Division of United Technologies has continued investigations of a configuration for a spaceborne laser radar (ladar) to meet the requirements for rendezvous and docking with a cooperative object in synchronous orbit.

The effort under this program consisted of an analysis of laser phase locking techniques, experimental verification of pulse repetition frequency (PRF) and resonant scanning control loops, and data measurements on a satellite mock-up.

The investigation supports the original contention that a rendezvous and docking ladar can be configured to offer a cost effective and reliable solution to envisioned space missions.

TABLE of CONTENTS

Section		Page
1.	INTRODUCTION	1-1
2.	SYSTEM REQUIREMENTS	2-1
2.1	Operation	2-1
2.2	Basic Configuration	2-1
2.3	System Block Diagram	2-1
3.	LASER CONTROL LOOP	3-1
3.1	Requirements	3-1
3.1.1	Offset Frequency	3-1
3.1.2	Transmitter PRF Control	3-1
3.2	Methods	3-2
3.2.1	Variation of Q - Switch	3-2
3.2.2	Variation of Laser Current	3-2
3.2.3	Variation of Laser Resonator Length	3-2
3.3	Configurations	3-4
3.4	Parameters of the Laser Components	3-4
3.5	Frequency Loop	3-6
3.6	PRF Loop	3-8
4.	LADAR EXPERIMENTAL INVESTIGATIONS	4-1
4.1	Experimental Set-up	4-1
4.1.1	Ladar Breadboard	4-1
4.1.2	Satellite Mock-up	4-3
4.1.3	Output Signals	4-3
4.1.4	Data Recording Equipment	4-4
4.2	Calibtation Experiments	4-6
4.2.1	Oscilloscope Amplitude Calibration	4-6
4.2.2	Retroreflector Return Calibration	4-8
4.2.3	Sphere Calibration	4-9
4.3	Initial Satellite Survey	4-9
4.4	Retroreflector Interaction Effects	4-11
4.5	Retroreflector Response Measuremtnts	4-13
4.6	Range Considerations	4-17
4.7	Final Satellite Survey	4-19
4.8	Summary	4-21

TABLE of CONTENTS (Continued)

APPENDICES		Page
A.	SCAN OPTIMIZATION	A-1
A.1	Summary	A-1
A.2	Description of the Four Line Scan	A-1
A.3	Power	A-1
A.4	Probability of Detection	A-2
A.5	Effective Probability of Detection	A-3
A.6	Scale Factor and PRF Versus Peak Power Trade-Off	A-4
A.7	Signal-to-noise Ratio	A-4
A.8	Probability of False Alarm	A-5
A.9	Results	A-5
B.	RANGE AMBIGUITY RESOLUTION by LASER PRF JITTER	B-1
B.1	Summary	B-1
B.2	Observation of Pulse Repition Interval (PRI) Jitter	B-1
B.3	Ranging Design	B-2
B.4	Analysis	B-2
B.5	Conclusion	B-4
C.	MAGNETIC TRANSDUCER	C-1
C.1	Introduction	C-1
C.2	Background an System Requirements	C-1
C.3	Disadvantages of PZT Transducers	C-2
C.4	Experimental Program	C-3
C.5	Design Effort	C-4
C.5.1	Hysteresis	C-4
C.5.2	Lateral Translation	C-5
C.5.3	Rotation About an Orthogonal Axis	C-6
C.5.4	Magnetic Efforts	C-8
C.5.5	Spring Material Considerations	C-9
D.	VIDEO TAPE OF LADAR EXPERIMENTS	
E.	COMPUTER MODELING OF DOUBLE CONTROL LOOP	E-1

LIST OF ILLUSTRATIONS

Figure		Page
1	System Block Diagram	2-3
2a.	Transmitter PRF versus Cavity Length	3-3
2b.	Frequency versus Cavity Length	3-3
3.	Laser Control Loop Diagram	3-5
4.	Response of PZT Transducer to a Unit Step Input	3-7
5.	Frequency Loop Block Diagram	3-7
6.	PRF Control Loop Block Diagram	3-9
7.	System Response to a Unit Step in PRF	3-9
8.	CO_2 LADAR Experimental System	4-2
9.	Baseline Satellite Mock-Up	4-4
10.	Ladar IF Output Signal	4-5
11.	Relative Amplitude Calibration of IF Output Signal	4-7
12.	Gain Correlation of IF Output Amplitude	4-8
13.	Calibration Sphere on Range Tower as Viewed from Ground at Range Tower	4-10
14.	Multiple Pulse IF Signal Encountered During Initial Satellite Survey	4-11
15.	Partial Multiple Pulse IF Signal Encountered During Initial Satellite Survey	4-12
16.	Return Pulse Amplitude as a Function of Rotation Angle	4-14
17.	Return Pulse Amplitude as a Function of Rotation Angle for Retroreflector With Cover Removed	4-15

LIST OF ILLUSTRATIONS (Continued)

Figure		Page
18.	Retroreflector Relative Power Response	4-16
19.	Predicted Retroreflector Relative Response	4-17
20.	Modified Retroreflectors Installed on Satellite Mock-Up	4-18
21.	Boom Suspended Satellite Mock-Up	4-19
22.	Alternate View of Boom Suspended Satellite Mock-Up	4-20
23.	Direct Photograph of Raster Scan Ladar Display	4-21
A-1	Four-Line Scan	A-2
A-2	Probability of Detection versus ϕ for S/N at Peak of Reference Beam = 8 dB	A-7
A-3	Probability of Detection versus k for S/N at Peak of Reference Beam = 8 dB	A-7
A-4	Probability of Detection versus ϕ for S/N at Peak of Reference Beam = 12 dB	A-8
A-5	Probability of Detection versus k for S/N at Peak of Reference Beam = 12 dB	A-8
A-6	Effective Power loss versus Phase Angle	A-9
A-7	Computer Program Listing (Superbasic)	A-10
C-1	Breadboard Magnetic Transducer	C-3
C-2	Laser Beam and Mirror Coordinate System	C-5
C-3	Transducer Mechanical Schematic Diagram	C-7
C-4	Magnetic Laser Mirror Transducer	C-9
E-1	CSMP Simulation Block Diagram	E-2
E-2	CSMP Program Implementing Block Diagram of Figure E-1	E-2

SECTION I
SUMMARY

Recent studies conducted under NASA auspices have established that (1) a pulsed coherent CO_2 ladar will offer a cost-effective and reliable solution to space rendezvous and docking requirements, and (2) the system configuration is capable of performance unattainable by any other means. By utilizing existing technology, it is possible to construct a 39 pound sensor that will be capable of detecting and tracking a passive cooperative target out to a range of greater than 600 nautical miles. The sensor is also capable of providing guidance for docking down to a range of several inches.

The studies were initiated under Contract NAS8-30738 and continued under Contract NAS8-31489. The following tasks were completed prior to the initiation of the current effort:

a. A baseline system was configured for an orderly growth from the present to anticipated 1985 technology. This system has been described in Norden Report 1247 R 0004.

b. A reflective optical design was accomplished. The design permits rapid and efficient beam scanning for search, as well as accurate beam positioning for tracking.

c. A coherent receiver utilizing a single four-quadrant detector array for search, acquisition, and track was designed.

d. The performance of the system was calculated and trade-off studies made to ensure that the system configuration was optimum with respect to size, weight, and power consumption.

In order to further support NASA in the development of the ladar sensor, Norden has accomplished three additional tasks under a continuation of Contract NAS8-31489. The tasks were specifically selected to confirm the analysis of sensor performance before initiating an engineering development phase. A brief description of the three tasks covered in this report are as follows:

1. Laser Control Loop - An analysis of techniques for phase locking of the transmitting laser with the local oscillator (LO), necessary to permit the pulse repetition frequency (PRF) to be controlled and synchronized with the resonant scanning mirror. This effort is detailed in Section 3.

2. Laser Control Loop Breadboard - Modification of the existing Norden ladar by adding a breadboard control loop, which is designed to confirm the calculations performed under the previous task. This effort is described in Section 4.1.

3. Measurements - Construction of a satellite mock-up and measurements to confirm the validity of the signal-to-noise and range calculations. This effort is described in Sections 4.2 and 4.3.

During the analysis of the laser control loop, the following items came to light which affect the baseline configuration:

a. Further trade-offs were required between scan pattern elemental coverage and PRF.

b. The techniques which were originally defined for the resolution of range ambiguities by controlling the PRF would have to be reexamined.

c. The bandwidth of the laser control loops is severely limited by internal resonances of the PZT transducers.

The scan pattern review, discussed in Appendix A, has resulted in new scan parameters which will ultimately yield the equivalent of 3 dB additional performance in target acquisition. In the configuration of the original scan pattern the beam illuminated each elemental area for exactly one pulse repetition period; the beamwidth was assumed to be the actual 3 dB beamwidth. Appendix A examines the alternative of single hit detection and of spreading the scan pattern for a lesser degree of beam overlap which lowers the pulse repetition rate and increases the peak pulse power. The probability of detection per frame was obtained for a point target, as a function of the degree of beam overlap and the phase angle of the scan mirror at the occurrence of a laser pulse. The trade-off curves of Appendix A indicate that a higher peak power and a lower PRF will ultimately yield an optimum configuration.

The investigation of PRF control, discussed in Appendix B, showed that a range ambiguity technique based on the natural pulse-to-pulse jitter of the transmitting laser should, when reduced to practice, be simpler and more cost effective to implement than the original design. The original technique had involved precise control of the transmitter PRF. It has been determined that the control will not be possible because the Q-switched laser pulses essentially build up out of noise and cannot be accurately controlled. However, subsequent measurements of the natural pulse-to-pulse jitter have shown that range ambiguities can be resolved by measuring the natural PRF variation, and implementing a range resolution algorithm.

When the laser breadboard was tested, it was found that the loop responses are in fact different from the calculated values. The variation in loop responses occurs because PZT units are in fact severely underdamped. In order to improve the loop responses, a magnetic device has been proposed to replace the PZT transducers. The device is more reliable, uses less power and is smaller and lighter than an equivalent PZT unit. In addition, the damping ratio of the magnetic unit is completely controllable by varying simple design parameters. Details of the magnetic laser transducers are contained in Appendix C.

The second task under this portion of Contract NAS8-31489 consisted of breadboarding the laser control loops which resulted from task 1. Several interesting results have been obtained from the breadboard. One of the most significant is that the pulsed transmitting laser must be used as the basic frequency reference, since the Q-switched laser pulses are built up out of noise. It is impossible to control the phase of such a pulse, because a good portion of the pulse has occurred by the time control can be initiated. Therefore, the loops were breadboarded using the pulsed transmitting laser as the frequency reference. Although the ladar performance was limited by the discriminator and PZT resonance considerations, the loops have been locked and heterodyne measurements accomplished. These breadboard results are discussed more fully in Section 4.1.

The third task consisted of a series of measurements on a target configured to simulate the optical signature of an actual spacecraft. The significant results of the measurements are as follows:

a. The cross-section of the spacecraft target was confirmed to be as predicted.

b. At certain target positions, specifically where an equal return was received from two adjacent retroreflectors, an interference pattern was detected.

c. Detection of a spinning spacecraft was confirmed as predicted.

The results and their impact on the system configuration are discussed in Sections 4.2 - 4.8.

SECTION 2
SYSTEM REQUIREMENTS

The ladar sensor system is configured to search, discriminate, acquire, track, and dock. Each of these functions presents a unique set of constraints on the output waveform and on the associated signal processing.

2.1 Operation

The sequential operation of the Ladar Space Rendezvous and Docking System is as follows:

a. Search - The system is pointed to the most probable target position and a search is initiated over a 5° by 5° sector.

b. Discrimination - The target of interest is separated from spurious targets and debris.

c. Acquisition - The target is acquired in angle and range.

d. Track - The target is tracked in angle and range, as the vehicle maneuvers into position for rendezvous.

e. Docking - The vehicle maneuvers into position to mate with the target.

2.2 Basic Configuration

The system is configured to utilize a passively Q-switched CO_2 laser as the transmitter and a four-quadrant photodiode detector as a coherent receiver. The laser and receiver configuration are similar to equipment which presently exists in a deployable form for airborne applications. The electronics, logic, and computer interface are similar to equipment which is associated with most coherent pulse-doppler radar sets.

2.3 System Block Diagram

A block diagram of the system is shown in Figure 1. The functional system operation is controlled by the on-board vehicle computer. The computer programs the modes of operation and performs calculations, such as ambiguity resolution

necessary for target tracking. The vehicle computer is also assumed to be available for several minor functions, such as closing the control loops for angle and range tracking, as well as for spurious target rejection.

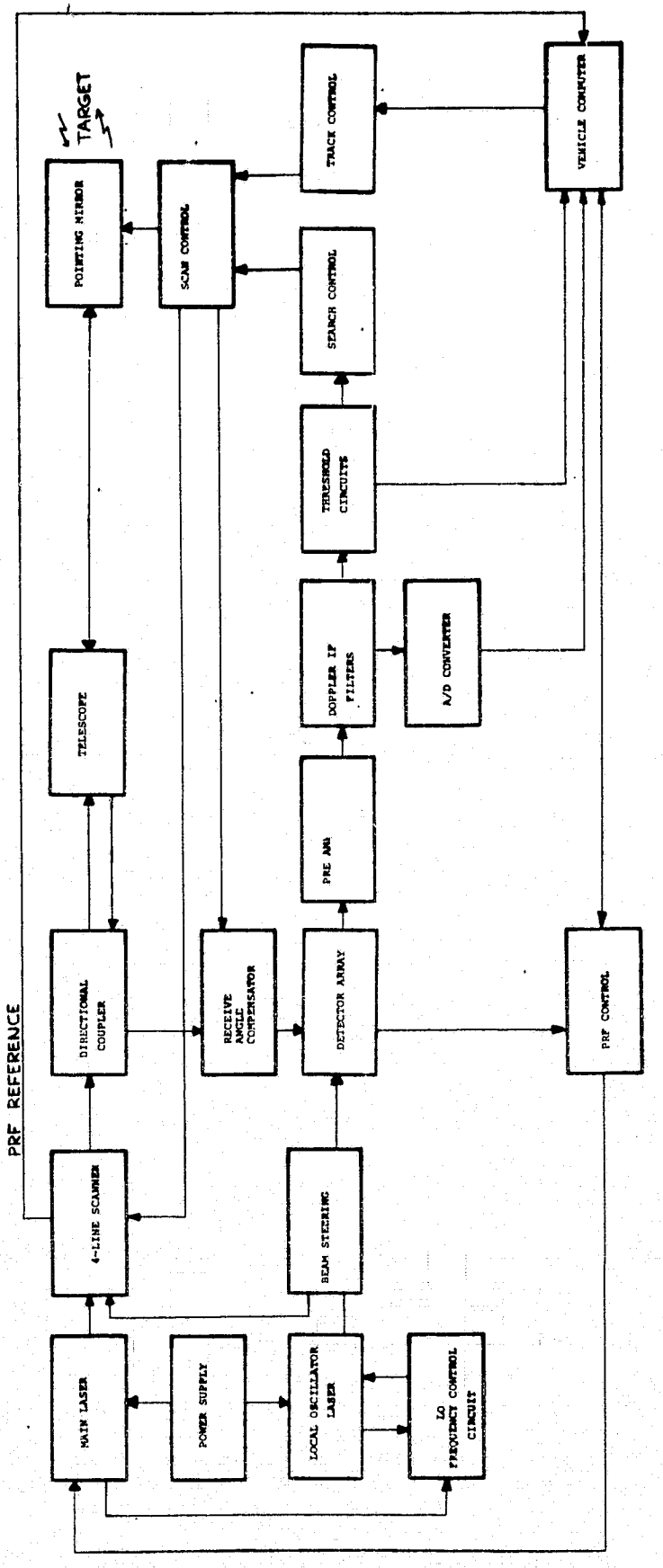

Figure 1. System Block Diagram

ORIGINAL PAGE IS
OF POOR QUALITY

SECTION 3
LASER CONTROL LOOP

The ladar described in the final report of Contract NAS8-30738 utilizes two lasers - a high-power pulsed transmitter and a low-power continuous-wave local oscillator (LO) - in the coherent transceiver to permit heterodyne detection of the signal returns. This section describes the first task under this portion of Contract NAS8-31489 a study of various techniques for PRF control and phase synchronizing of the lasers to permit coherent detection in an efficient manner.

3.1 Requirements

3.1.1 Offset Frequency

In order to minimize the bandwidth of the receiver doppler filters and therefore to maximize detected signal-to-noise, it is necessary to operate at a fixed IF (intermediate frequency). The requirement is equivalent to that of a fixed frequency offset between the transmitting and LO lasers. Therefore, one of the lasers must be injection locked to the other.

3.1.2 Transmitter PRF Control

Precision ranging to the target satellite requires a controlled variation of the transmitter PRF to resolve range ambiguity. In Section 5.3.7 of report 1247 R 0004 a design was proposed in which the range ambiguity could be resolved by forcing the PRF sequentially to assume two precisely controlled values.

Measurements performed during the present work have shown, however, that a precise control of the PRF is not obtained. The control loop maintains the time average of the PRF at the desired value, which insures synchronization with the mirror scan, while the individual pulse repetition intervals are subject to a small random jitter. A method of range ambiguity resolution which takes advantage of this fact is proposed and analyzed in Appendix B.

3.2 Methods

3.2.1 Variation of Q-Switch

Since the transmitter pulsing is accomplished by means of an intra-cavity SF_6 passive Q-switch, the PRF could be varied by changing the gas pressure in the cell. Qualitatively, the PRF is inversely proportional to cell gas pressure; laser technology constraints, however, dictate the use of a static cell pressure for single mode (TEM_{∞}) frequency operation.

3.2.2 Variation of Laser Current

Changes in the laser tube discharge current result in plasma density changes which affect the index of refraction in, and the optical length of, the laser cavity. The net effect is a change in the laser frequency as well as, in the case of the transmitter, a change in the PRF.

The control method has a very high response bandwidth which is not limited by mechanical resonance. The control range, however, is typically limited to ±4 MHz in frequency and ±5 kHz in PRF. Since these control ranges are inadequate, the approach will not be considered further.

3.2.3 Variation of Laser Resonator Length

The PRF of the transmitter can also be controlled, as can the laser frequency, by changes in the length of the laser resonating cavity. As the cavity length is modulated, the laser frequency varies within the constraints of the P_{20} laser line while the PRF varies over a dynamic range of approximately 3:1. Figure 2 illustrates how the PRF and the frequency are both functions of the laser cavity length.

Cavity control can be implemented electro-mechanically by a transducer (e.g., a PZT crystal holding one of the laser mirrors) driven by an amplifier whose input is an appropriate error signal in the control loop. Control bandwidths are limited by the resonant frequency of the transducer; the typical PZT mirror system bandwidth is 0.5 to 2 kHz. Appendix C describes a magnetic transducer with a wider bandwidth response which could replace the present PZT devices.

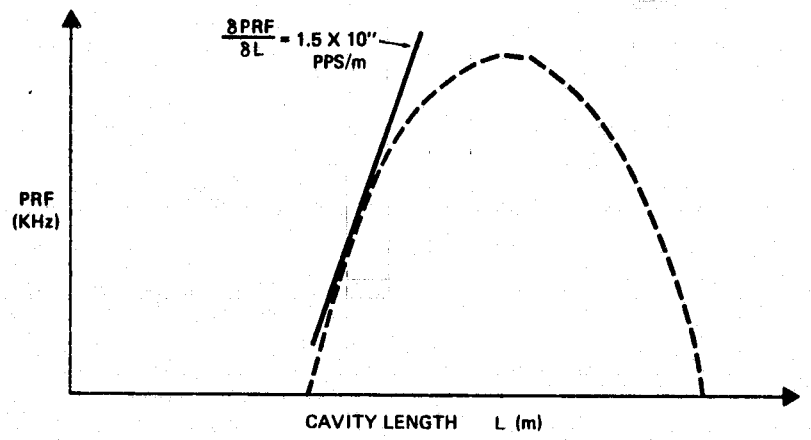

Figure 2a. Transmitter PRF versus Cavity Length

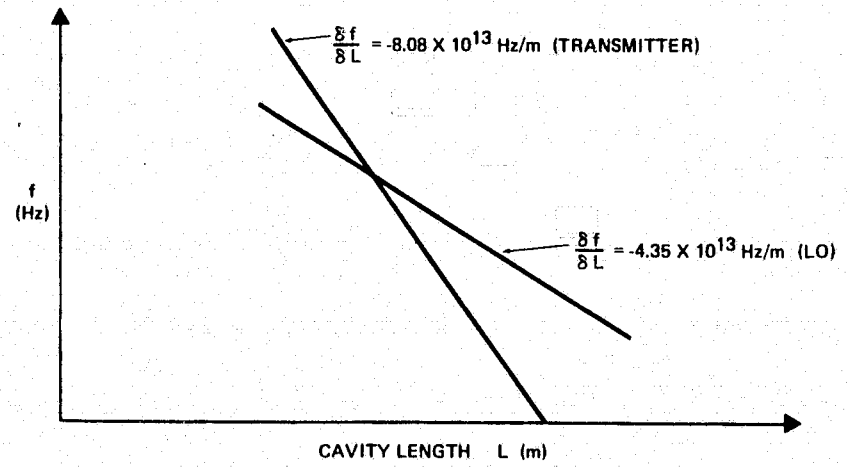

Figure 2b. Frequency versus Cavity Length

3.3 Configuration

The control configuration used in the breadboard is depicted in the block diagram of Figure 3. The transmitter is used as the frequency reference with a PRF control signal used to drive the PZT controlling its cavity length. In the double-loop control system shown, the absolute values of the two laser frequencies, which are separated by the required offset frequency, shift in order to operate at the prescribed PRF. Locking of the control loop is facilitated and frequency mode hopping is inhibited, since the transmitter is equipped with a reflective grating to select the desired lasing line.

A similar configuration with the transmitter and LO lasers interchanged is possible; i.e., where the LO is used as the reference for frequency control. Since the spacing between lasing lines is larger in the shorter LO laser, the two configurations are, in effect, functionally equivalent.

The design of the control loop is essentially the same for either one of the configurations. The analysis and simulation below considers the transmitter as the reference for frequency control. The control loop should be designed to be slightly underdamped. A track filter with a frequency cut-off lower than the resonant peak of the (PZT) transducer is used and the loop gain adjusted to achieve the desired damping characteristics.

3.4 Parameters of the Laser Components

As shown in Figure 2, the laser parameters of interest are the following:

	Transmitter	LO
Length (m)	0.65	0.35
Frequency sensitivity to length changes (Hz/m)	-4.35×10^{13}	-8.0×10^{13}
PRF sensitivity to length changes (pps/m) at 25000 pps	1.5×10^{11}	-

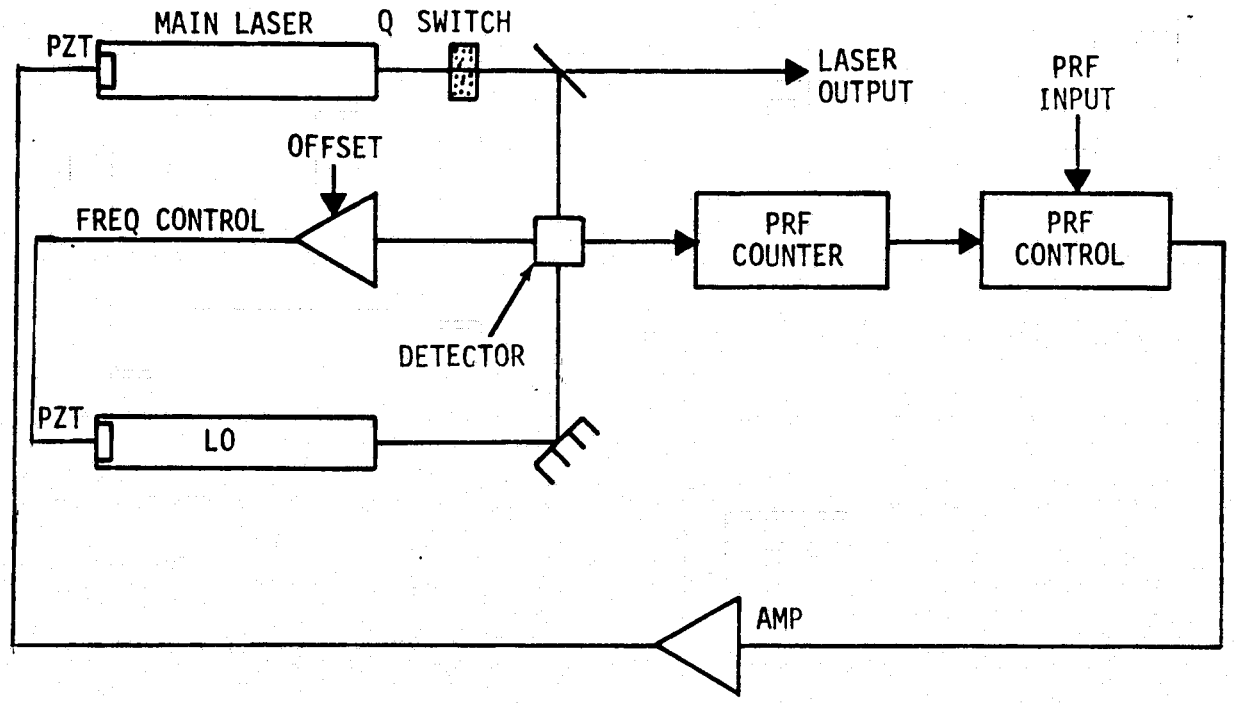

Figure 3. Laser Control Loop Diagram

The transformer (PZT crystal and mirror combination) constitutes an underdamped electro-mechanical system which can be described by the following transfer function normalized for unity response at a DC gain of 10^{-8} m/volt:

$$A(s) = \frac{\omega_o^2}{s^2+2\zeta\omega_0 s+\omega_o^2} \quad , \text{ where}$$

ω_o is the resonant frequency of 15,716 rad/sec (2500 Hz), and

ζ is a damping factor of 0.167.

The response of the undamped and damped transducer to a unit step input is shown in Figure 4.

3.5 Frequency Loop

As discussed above, the configuration is based on the use of a low-pass filter and integrator to damp the PZT transducer of the laser cavity, with the control loop having a damping ratio of 0.7.

The control system design proceeded in a manner which separated the dynamics of each of the loop control functions. The control signal in each of the laser loops causes a change in the linear dimension of the PZT transducer; this variation changes the resonance of the laser cavity which, in turn, shifts the frequency. The grating within the transmitter cavity ensures that lasing can only occur on the P_{20} transition. The PRF is a function of the properties of the Q-switch, and with the Q-switch fixed, varies with the exact lasing wavelength within the P_{20} transition. The control loop illustrated in Figure 5 shows a compensation circuit with a cut-off frequency of 1000 Hz; it is slightly underdamped for a gain of $K = 1.86 \times 10^7$. The corresponding loop transfer function used in Figure 6 is

$$T(s) = \frac{4.6 \times 10^{15}}{[(s+3191)^2+(3177)^2][(s+2568)^2+(1485)^2]}$$

The response of the loop to a unit step function input has a 4% overshoot and settles within 1% of its final value in 1.5 ms.

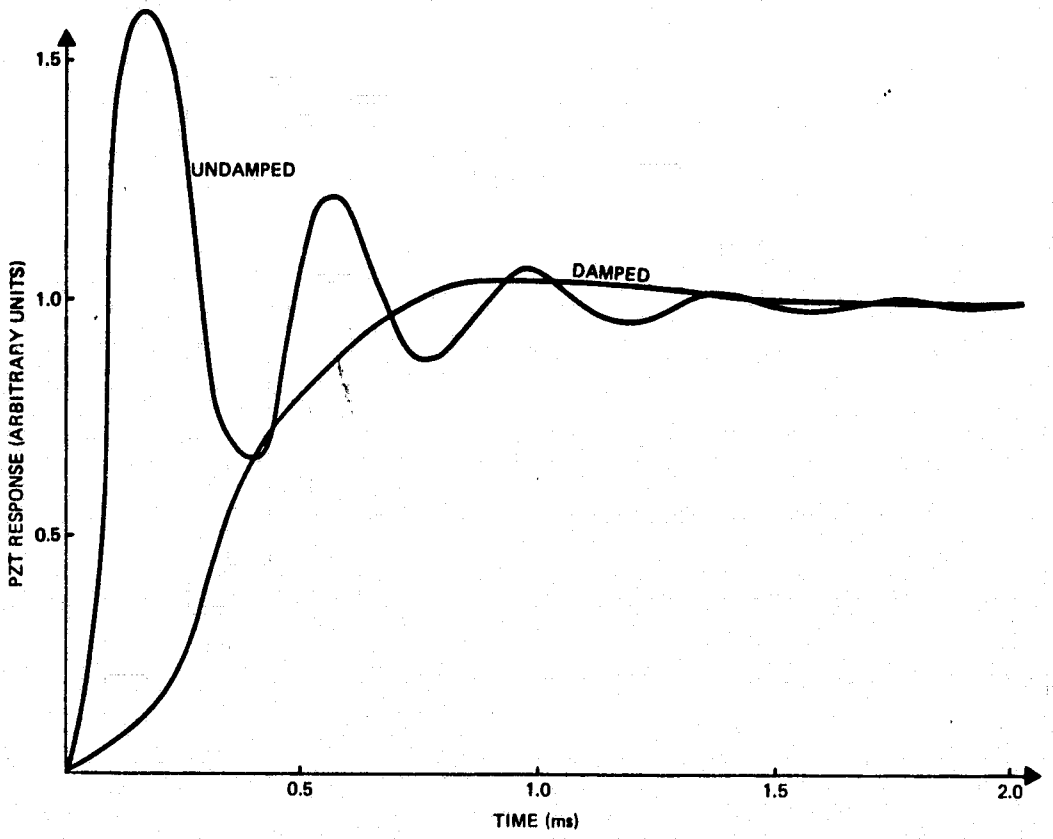

Figure 4. Response of PZT Transducer to A Unit Step Input

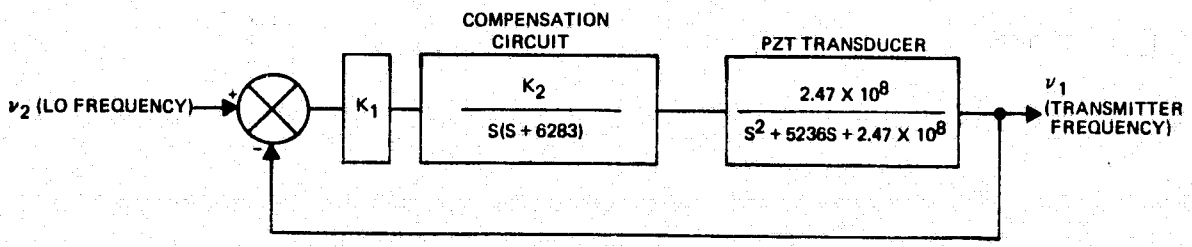

Figure 5. Frequency Loop Block Diagram (Damped PZT Transducer)

3.6 PRF Loop

When included in the double-loop configuration of Figure 3, the frequency loop of Figure 5 gives rise to the block diagram of Figure 6. A cut-off frequency of ω_c = 15,000 rad/sec was selected as was a gain of K = 0.13 yielding a unit step response time of 3.4 ms for an absolute error value less than 0.01. Since the ladar sensor optimum performance is not very sensitive to the phase angle (see Appendix A, Figure A-3), this means that system noise has no practical effect on the performance.

The system response to a unit input step in PRF, simulated by a Computer System Modeling Program (CSMP) (see Appendix E) is displayed in Figure 7. The results indicate stable operation and also reveal that the phase error between the laser pulses and the oscillating scan mirror is below 10° within 4.2 ms.

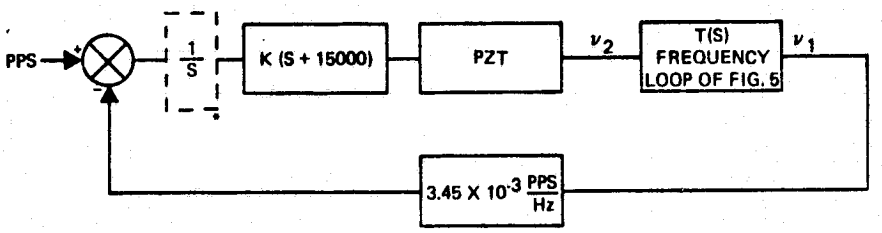

* THIS INTEGRATOR IS IMPLICIT IN THE READING OF PHASE INSTEAD OF FREQUENCY, AND NEED NOT BE PHYSICALLY IMPLEMENTED.

Figure 6. PRF Control Loop Block Diagram

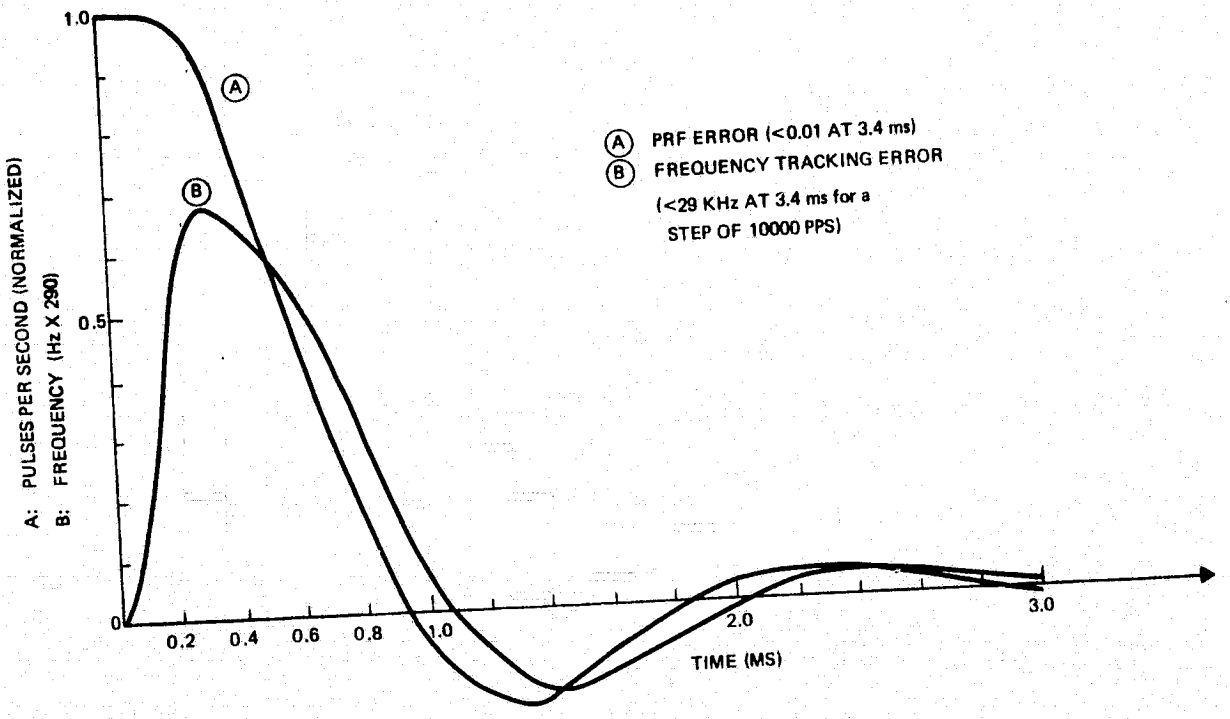

Figure 7. System Response to a Unit Step in PRF

SECTION 4
LADAR EXPERIMENTAL INVESTIGATIONS

In order to provide design guidance and confirmation for the icosahedron satellite retroreflector configuration, a number of experimental investigations were undertaken. Using the previously developed Norden coherent ladar breadboard unit, the characteristics of individual retroreflectors and a satellite mock-up were determined. Coherent beam subtraction effects, individual unit variations, and response as a function of satellite orientation were also studied.

4.1 Experimental Set-up

The set-up for the experimental investigation consisted of the Norden coherent ladar unit and an icosahedron array of retroreflectors on a satellite mock-up. The satellite was located at a range of 695 m which corresponded to the distance of the Norden radar test range tower from the ladar laboratory. Further details of the ladar breadboard, satellite mock-up, various output signals, and data recording equipment are discussed below.

4.1.1 Ladar Breadboard

The ladar transceiver used in these investigations is a pulsed, coherent laser radar operating at a wavelength of 10.6 micrometers with a PRF of approximately 32kHz. An average output power of approximately 0.7 Watt consisting of pulses with 280×10^{-9} sec FWHM (full width, half maximum) pulsewidths delivers peak pulse powers of 78 Watts. The divergence of the transmitted beam was measured to be approximately 0.5 milliradians (mr) at the 50% power points. The divergence was measured by determining the profile of the beam at the 695 m range.

A block diagram of the CO_2 ladar transceiver is shown in Figure 8. The system, including the capability of PRF locking to an independent high frequency scanning mirror, has been described in previous reports; however, the basic features are repeated here for clarity.

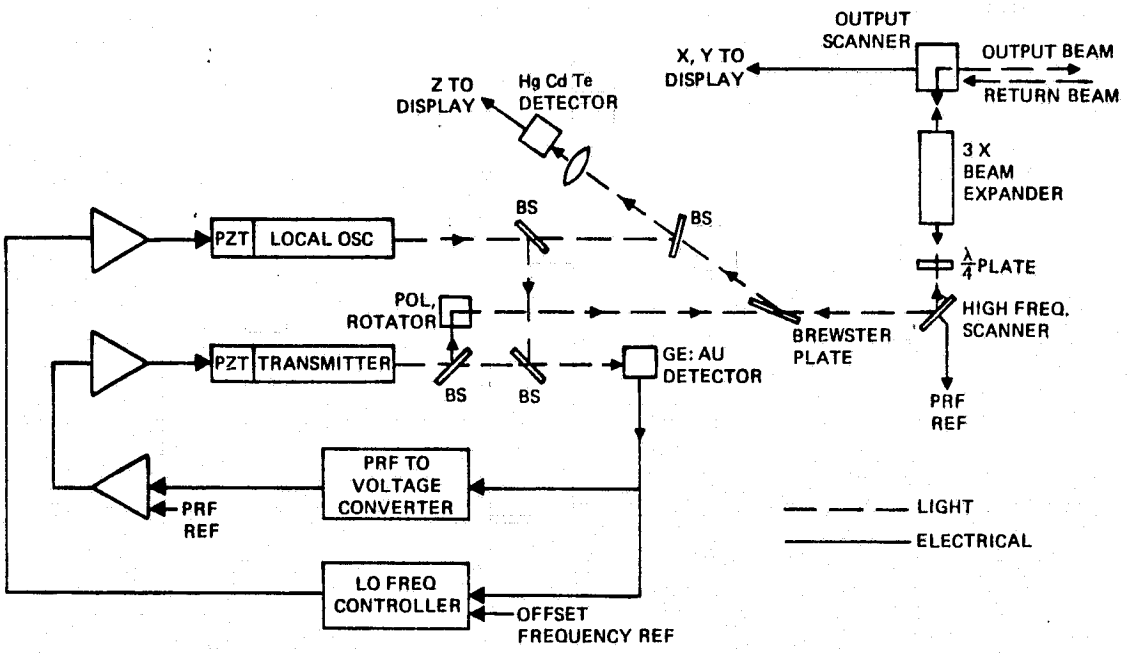

Figure 8. CO_2 Ladar Experimental System

The PRF is compared to either an internal reference signal or a phase comparison signal from an external high frequency scanning mirror -- a resonant device of essentially constant frequency. The control signal resulting from the PRF comparison is used to vary the PZT mirror tuning element on the transmitting laser which, in combination with an intra-cavity saturable absorber cell, changes the PRF to coincide with the desired PRF. The saturable absorber cell control of the PRF also stabilizes the output frequency of the transmitter laser. The heterodyne signal from a Ge:Au detector provides an offset signal which is the difference frequency between the transmitter and LO lasers. The signal is used to vary the LO PZT mirror tuning element to change the LO frequency offset to match the center frequency of the ladar receiver IF strip.

The majority of the laser transmitter output beam is rotated in polarization, directed through the Brewster plate polarization separator, reflected from the high frequency scanning mirror, changed to circular polarization by a 1/4 wave plate, beam expanded by a 3X Galilean telescope, and reflected out of the transceiver by a pair of galvanometer scanned mirrors which are synchronized to the transmitter PRF.

The return signal from a specular target will first retrace the output beam path through the scanner and beam expander. In returning though the 1/4 wave plate, however, the beam experiences an additional 1/4 wave of retardation and becomes linearly polarized in a direction which is orthogonal to the original polarization. The returning polarization rotated beam is, therefore, reflected by the Brewster plate polarization separator. The separated return beam is subsequently mixed with the LO beam by means of a beam splitter and the overlapped beams are focused onto the face of the 39% quantum efficiency HgCdTe detector.

The detected RF difference frequency (approximately 15 MHz) is amplified, range gate controlled, and either directly monitored or used to control the Z-axis intensity of an oscilloscope. The X and Y axes of the latter are controlled by position signals from the galvanometer scanning mirrors to produce a radartype raster scan. The gain of the IF amplifier can be varied in order to reduce the transceivers sensitivity to strong signal returns and hence prevent saturation of the amplifier when comparison measurements are required.

4.1.2 Satellite Mock-Up

The icosahedron retroreflector array was fabricated by mounting twenty commercially obtained retroreflector assemblies around the periphery of a cylinder as illustrated in Figure 9. As can be seen in the figure, the tilt of the retroreflectors relative to the satellite axis was provided by mounting blocks.

The individual retroreflectors used were received from the vendor with protective "cans" around them to protect the sharp outer edges of the units from accidental damage as well as the handling personnel from injury. A more detailed discussion of the packaging configuration is contained in a later section.

4.1.3 Output Signals

A number of different output signals were available to provide information about, and characteristics of, the return signal. The radar type raster scan (mentioned in Section 4.1) uses the return signal to modulate the intensity of an oscilloscope display and the galvanometer scanning mirror positions to control the X and Y beam positions of the display. For the 32kHz PRF and an 512 x 512 element display, approximately 8 seconds are required to scan one frame of data.

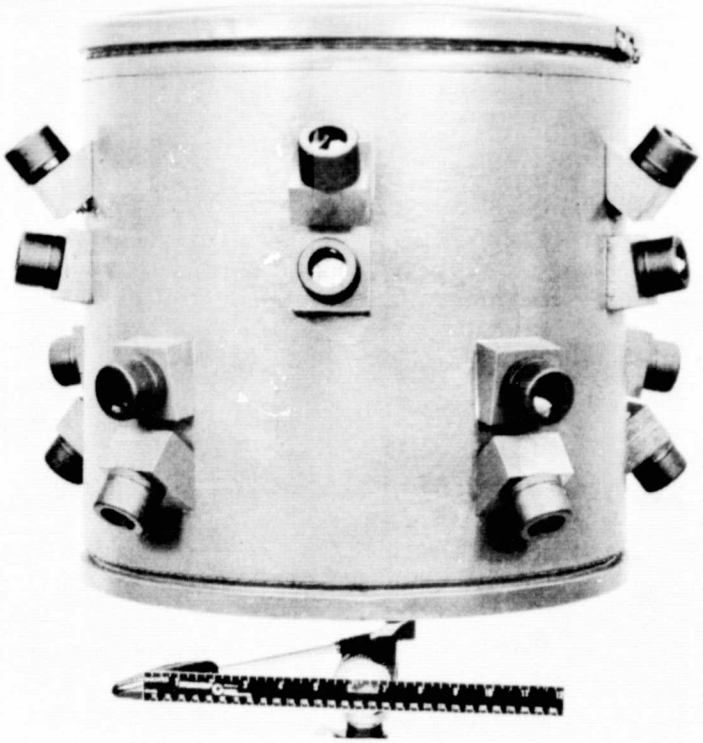

Figure 9. Baseline "Satellite Mock-Up"

Another type of output signal is obtained by displaying, in real time, the IF output signal as illustrated in Figure 10. In this display of repetitive pulses, the small pulse at the left of the scan is the feed-thru pulse of the transmitter main bang. Although range gating of the IF amplifier gain is employed, a small amount of the main bang signal was still detected; the source is believed to be scatter and reflections from the optical surfaces of the beam expanding telescope. In Figure 10 the return signal from a single retroreflector is displayed just to the right of the center of the screen. The IF amplifier gain has been adjusted in this case to provide 5 divisions of vertical amplitude -- which is just below where the amplifier begins to saturate with increased input signal. For this type of data the transceiver was not scanned; the beam location was adjusted to continuously point at the target. Most calibration measurements were made from this type of data display.

4.1.4 Data Recording Equipment

In addition to notebook data of the observed target return pulse amplitudes, two types of data recording equipment were used in the experiments. The first was conventional photographic recording of the data displays with an oscilloscope camera.

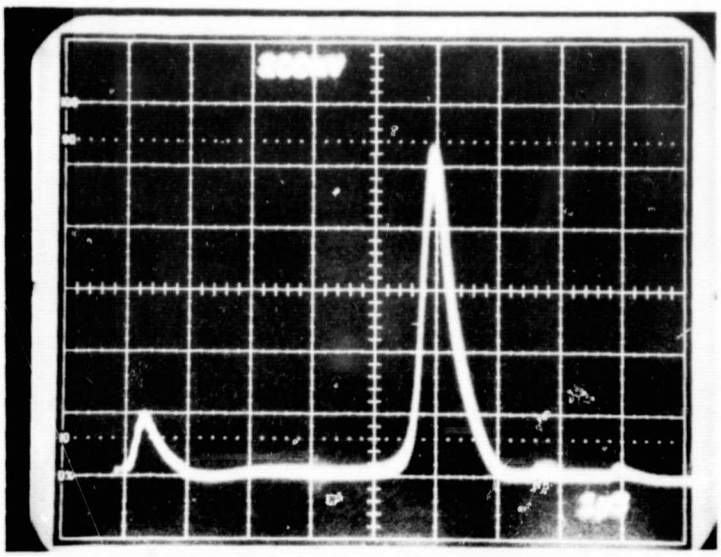

Figure 10. Ladar IF Output Signal

The second, and more versatile technique, was to videotape the data displays as they occurred in real time for later study and analysis. The recording was carried out by detecting the display information with a Concorde Model TCM-55 TV camera and recording the information on a Sony Model VO-2800 videotape recorder. This allowed the ladar scanning information to be recorded and later analyzed on a frame-by-frame basis, if necessary. Also possible was a continuous display of the retroreflector return signal as the satellite mock-up was rotated.

The availability of the TV camera and videotape recording equipment also permitted recording of the satellite mock-up rotation rate as seen from the ladar transceiver location. In this case recording was accomplished with the aid of a Questar astronomical telescope, previously modified to adapt to the TV camera. The latter type of recordings clearly show the heat wave or "mirage" effects of the atmosphere over the 695 m range: the effect may of course be substantially different at the 10.6 μ wavelength.

4.2 Calibration Experiments

In preparing to conduct experiments with the satellite mock-up, it was desired to have

a. a calibration of the IF output amplitude (such as Figure 10) as a function of input signal power and/or attenuation

b. a measure of the signal strength of a single retroreflector compared to the background noise level (maximum signal-to-noise ratio)

c. a check of system sensitivity by determining the signal return from a 0.508m (20 inch) diameter calibration sphere.

Because of atmospheric fluctuations and distortions which change rapidly with time, the average amplitudes during the tests were necessarily estimated by eye from the oscilloscope screen. The tests do serve, however, to determine the magnitudes of the various interactions and effects. The results of the calibration experiments are presented in the following sections.

4.2.1 Oscilloscope Amplitude Calibration

The IF output amplitude display (see Figure 10) provides a measure of the strength of the target return signal. It was desired to provide a relative calibration of the oscilloscope display in order that target returns under varying conditions might be compared.

Calibration was carried out by observing the amplitude decrease associated with rotating the 1/4 wave plate from its normal orientation (which yields a complete polarization rotation of 90° as a result of two passes of phase retardation) to an effective 1/8 wave plate orientation (which yields circular polarization as a result of two passes). The net result is a comparison of full transmission and 3dB optical power attenuation conditions. The comparison was made for varying amplitudes of signal return by adjusting the scanning mirrors to produce the desired full transmission return. The maximum display amplitude was normalized to approximately five divisions which appeared to be the threshold level for saturation effects. A plot of display amplitude as a function of attenuation for low and high IF gain conditions is presented in Figure 11.

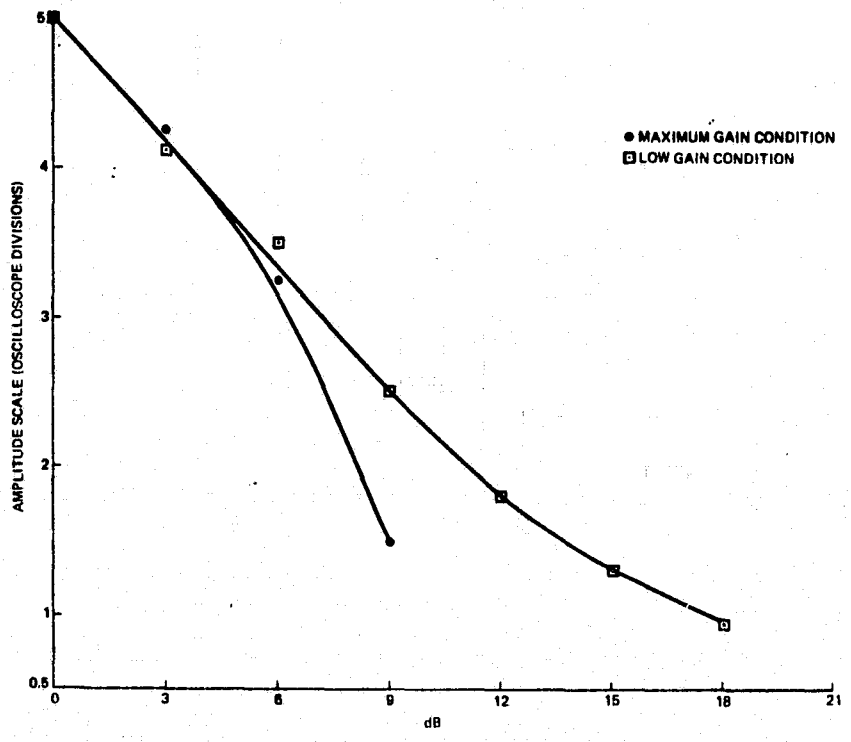

Figure 11. Relative Amplitude Calibration of IF Output Signal

In addition to the variation in the signal return from target cross section, the display amplitude may be varied by means of an attenuator in the IF amplifier. In order to determine the oscilloscope amplitude calibration with respect to the IF attenuator setting, a comparison of amplitude versus optical attenuation was made for the low and high gain settings of the IF amplifier. The optical attenuation was accomplished by rotating the 1/4 wave plate from its maximum to its minimum transmission orientations. The correlation between low and high gain settings of the amplifier is shown in Figure 12.

The data used in Figure 11 was subjected to a least squares curve fitting analysis. It was found that all but the two maximum amplitude data points fit a square root power law curve; this may be contrasted to the linear behavior which is typical of an isolated photodetector. The power law response is believed to result from the attenuator circuit in the IF amplifier. The circuit utilizes a variable bias applied to a shunting diode in order to vary the attenuation of the diode and hence the gain of the amplifier. The model also explains the much lower amplitude of the 9 dB data point for the maximum gain condition. That is,

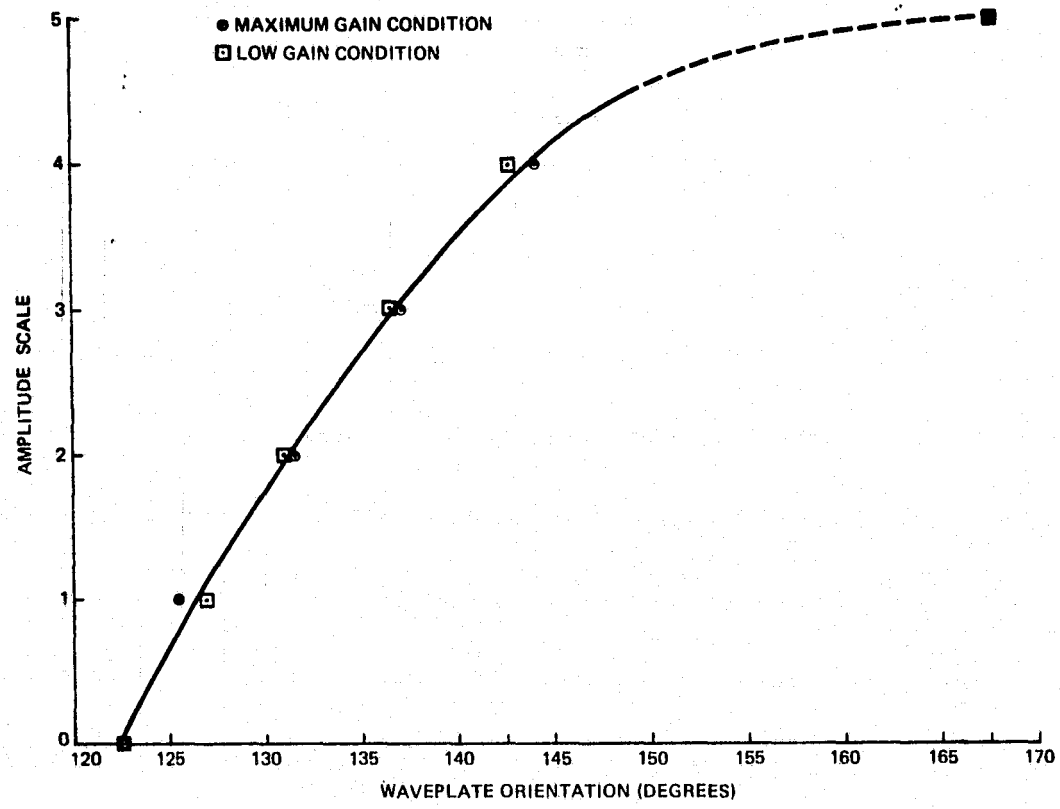

Figure 12. Gain Correlation of IF Output Amplitude

when the signal level is smaller than the junction potential of the diode, then the diode attenuation characteristic is effectively out of the circuit. The not quite perfect fit of the power law curve for the maximum amplitude data is believed to result from the onset of saturation of the amplifier. As noted earlier, the five division amplitude was selected because it appeared to be below saturation. This was, however, a visual estimate of the display and hence it is quite possible that a small amount of saturation was occuring.

4.2.2 Retroreflector Return Calibration

In order to determine the signal level of the retroreflector return relative to the noise level of the present ladar transceiver, a second calibration measurement was made. In this measurement dielectric coated Germanium mirrors were introduced into the transmit and return signal paths to reduce the amplitude of the retroreflector return signal to the transceiver's noise level. It was found that simultaneously introducing 90%, 80%, and 65% reflectivity mirrors (which have 9.6%, 27%, and 33%

transmissions, respectively) gave a return signal which was slightly above the system noise level. Since the three mirrors were introduced into the optical beam at a location which was common to both the transmit and receive paths, the retroreflector return signal is approximately 42 dB above the noise level of the system. It should be noted that this signal-to-noise ratio is only applicable to IF output display observations. In the Z-axis modulation raster display and other representations, the signal-to-noise ratio may be determined by other factors, such as incomplete blanking of the transmitted pulse.

4.2.3 Sphere Calibration

In the preceding section the return signal was compared to the transceiver noise level -- a relative measurement. It was desired to also have a comparison to a target having a measurable cross section. For this test a specially fabricated 0.508 m (20 inch) diameter calibration sphere was used as the target. The calibration sphere consisted of a finely machined (63 micro-inch) hollow aluminum ball with a reinforced threaded hole to allow suspension of the sphere in free space. A photograph of the suspended calibration sphere appears in Figure 13.

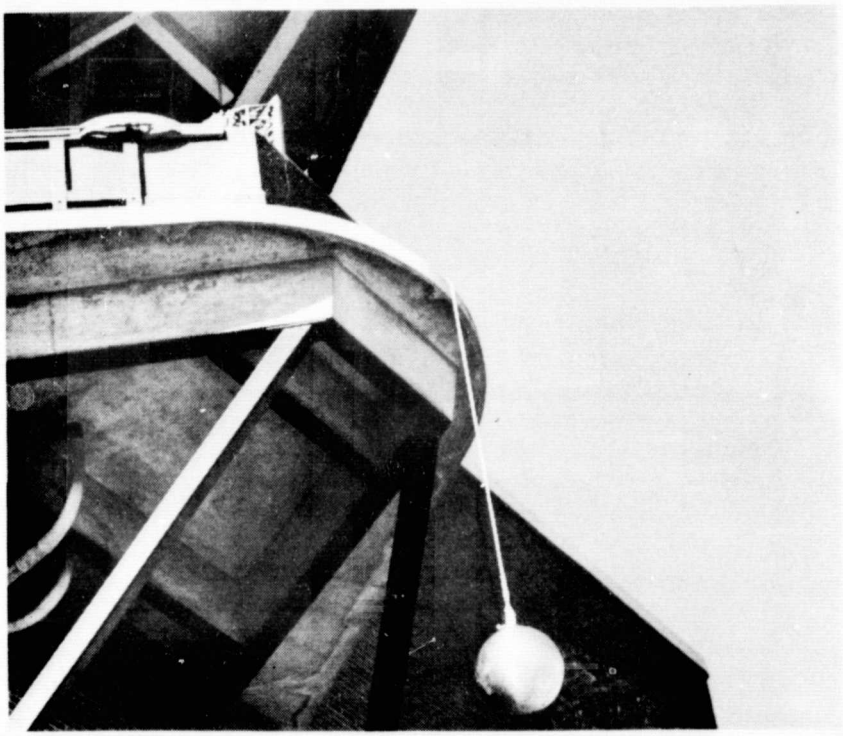

Figure 13. Calibration Sphere on Range Tower as Viewed From Ground at Range Tower

The return signal from the calibration sphere was found to be approximately equal to the ladar transceiver noise level. Thus, for the balance of the tests to be described in this report, the maximum sensitivity is equal to the cross section of the calibration sphere.

It should be noted that the cross-section sensitivity measured above is not the best which has been observed with the ladar system. Previous tests accomplished with a better HgCdTe detector were able to detect a smaller 0.15 m (6 inch) diameter polished steel sphere calibration target. A larger beam expanding telescope, such as would be used in an actual rendezvous sensor, would also increase the transceiver sensitivity by more than an order of magnitude.

4.3 Initial Satellite Survey

To determine the range of signal variations and checkout the satellite mock-up fabrication and assembly, an initial survey of the signal returns from the mock-up was made. To accomplish this survey the mock-up was mounted on a tripod (Figure 9) and the unit rotated about the axis of the satellite cylinder while the return signal was monitored. The initial survey identified two significant effects.

The first effect noticed was that the repetitive display of the signal return did not remain a single, clean pulse in all sectors of rotation. That is, the repetitive single-pulse return shown in Figure 10 becomes a multiple or "fuzzy" pulse during repetitive oscilloscope sweeps as shown in Figure 14. The variations from single to multiple return appeared to occur more or less regularly with continued rotation of the satellite mock-up. A more detailed investigation of this effect was subsequently undertaken and is reported in the following section on retroreflector interaction effects.

The second effect noticed during the initial survey was that, for satellite orientations (tilted axis) which did not yield the single to multiple pulse variations, the return signal decreased at locations of the rotation to a "null" or zero signal-level return. Further investigations and resolution of these problems are reported in Section 4.5 on Retroreflector Response Measurements.

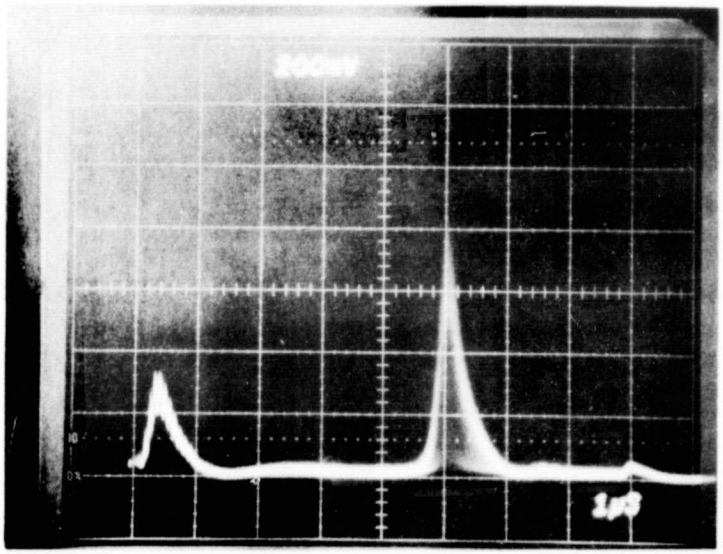

Figure 14. Multiple Pulse IF Signal Encountered During Initial Satellite Survey

4.4 Retroreflector Interaction Effects

As noted above, the initial survey observed more or less periodic changes in the return pulse amplitude as the satellite mock-up was rotated about its cylindical axis. The variation in return signal was between the smooth single pulse type of return typified by Figure 10 and the multiple or "fuzzy" pulse return typified by Figure 14. In changing from the single to multiple pulse nature, the single pulse would slowly decrease in amplitude, become partially multiple as illustrated in Figure 15, and finally become the full multiple pulse of Figure 14. As rotation of the mock-up was continued, the process was reversed until the full single pulse of Figure 10 was again obtained.

The first test conducted was to determine the period of the repeating single and multiple pulse behavior. The satellite mock-up was rotated through 360 degrees and the number of peaks, or single pulse returns, and nulls, or multiple pulse returns, was observed. It was found that 10 peaks and 10 nulls occured during the 360 degree rotation. Thus, the peak-to-peak signal rotation angle was 36° and the peak-to-null rotation angle was 18°.

The angular spacing between the peak (single pulse) signals corresponds to the spacing between the 10 retroreflectors seen as the satellite is rotated (while the ladar is illuminating the satellite normal to the axis of the satellite cylinder.)

Because of the period of the occurance of the null (multiple pulse) behavior, it was postulated that the behavior was a result of constructive and destructive interference between the returns from two simultaneously viewed retroreflectors. Therefore, the peak (single pulse) return would occur only when a single retroreflector's field-of-view was being illuminated by the ladar.

The constructive and destructive interference hypothesis was confirmed by repeating the rotating satellite measurements with only one set of circumferential retroreflectors active and the other three sets covered. The result was that only peak (single pulse) type of behavior was observed. As the satellite mock-up was rotated the pulse amplitude would decrease until no return was observed. As the rotation was continued, eventually another small pulse would appear and increase in amplitude to a peak.

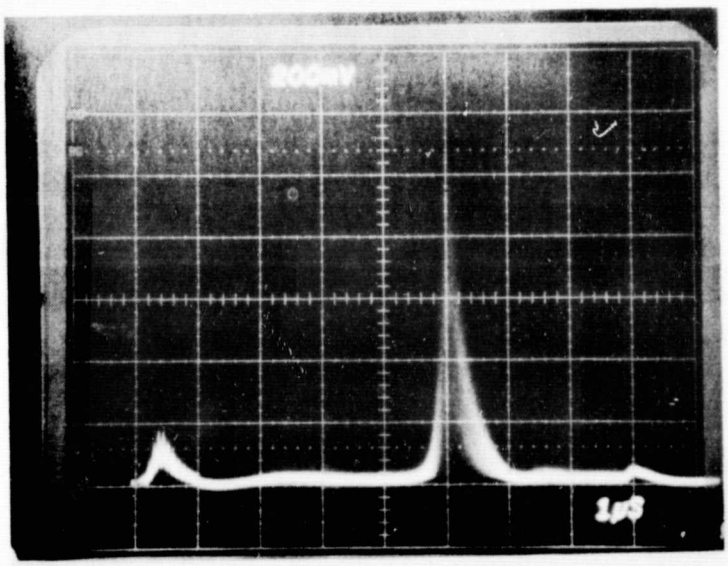

Figure 15. Partial Multiple Pulse IF Signal Encountered During Initial Satellite Survey

Further confirmation of the interference hypothesis was obtained by placing the (non-rotating) satellite in an orientation which gave a strong multiple pulse type of return. In this orientation first one and then the other of the two interfering retroreflectors was covered and the resulting return observed. It was found that blocking one retroreflector led to a stable single pulse type return which was approximately the mean of the multiple pulse return. That is, a multiple pulse return which yielded a "fuzzy" pulse extending from approximately 0 to 4 amplitude divisions would yield a single pulse type of return of 2 amplitude divisions when either of the two interfering retroreflectors was blocked. Thus the constructive interference of two amplitude division signals is 4 divisions while destructive interference leads to 0 divisions.

The rapid fluctuation in amplitude of two interfering signals contributing to the multiple pulse type return of Figure 14 is believed to result from atmospheric fluctuations. "Heat waves" are readily apparent in TV recordings taken through a high power telescope looking over the test range. The changes in the atmosphere cause the path length to (or speckle pattern from) the two reflectors to rapidly fluctuate. The rapid fluctuation leads to the "fuzzy" looking pulse of Figure 14. Although rapid atmospheric fluctuations will not be present in extraterrestrial applications of the ladar, the possibility of constructive and destructive interference between multiple retroreflector returns must still be considered. The answer to whether destructive interference will be a problem in satellite acquisition lies in analysing the rotation rate of the satellite relative to the ladar viewing direction during the acquisition period. Subsequent testing reported in the final satellite survey of Section 4.7 attempts to test the difficulty of acquisition for the terrestrial environment case.

It should be noted that the interaction of three retroreflectors, as a test of multi-element interactions, was also examined. Essentially the same interference effects were obtained for the three retroreflector case. The effects and ramifications of larger numbers of interacting retroreflectors were not studied at this time.

4.5 Retroreflector Response Measurements

The initial satellite survey and retroreflector interaction effects studies found that the various pairs of retroreflectors on the satellite mock-up did not appear to have as wide an angular coverage as expected. In particular, when the cylinder axis of the mock-up was tilted to block all but one row of retro-

reflectors, the signal return dropped to essentially zero at times during rotation. The loss of signal condition was not in agreement with predictions based on the expected field-of-view for individual reflectors in this configuration.

In order to clarify the angular coverage discrepancy, measurements of the field-of-view of an individual retroreflector were made. The unit tested was from the same vendor production lot as the units shown in Figure 9. The single retroreflector was mounted on a tripod whose rotating head gearing system had been previously calibrated. The return pulse amplitude as a function of relative rotation angle is plotted in Figure 16. It must be remembered that the pulse amplitude display is a non-linear function as pointed out in the section on calibration experiments. The field-of-view of the single unit is approximately 45° between the 10% amplitude points. Since, for some locations, the adjacent retroreflectors are 72° apart around the circumference of the satellite mock-up, this is definitely in keeping with the signal loss observations. It was then necessary to determine the source of the difference between the original field-of-view estimate for the retroreflectors and that which was actually measured.

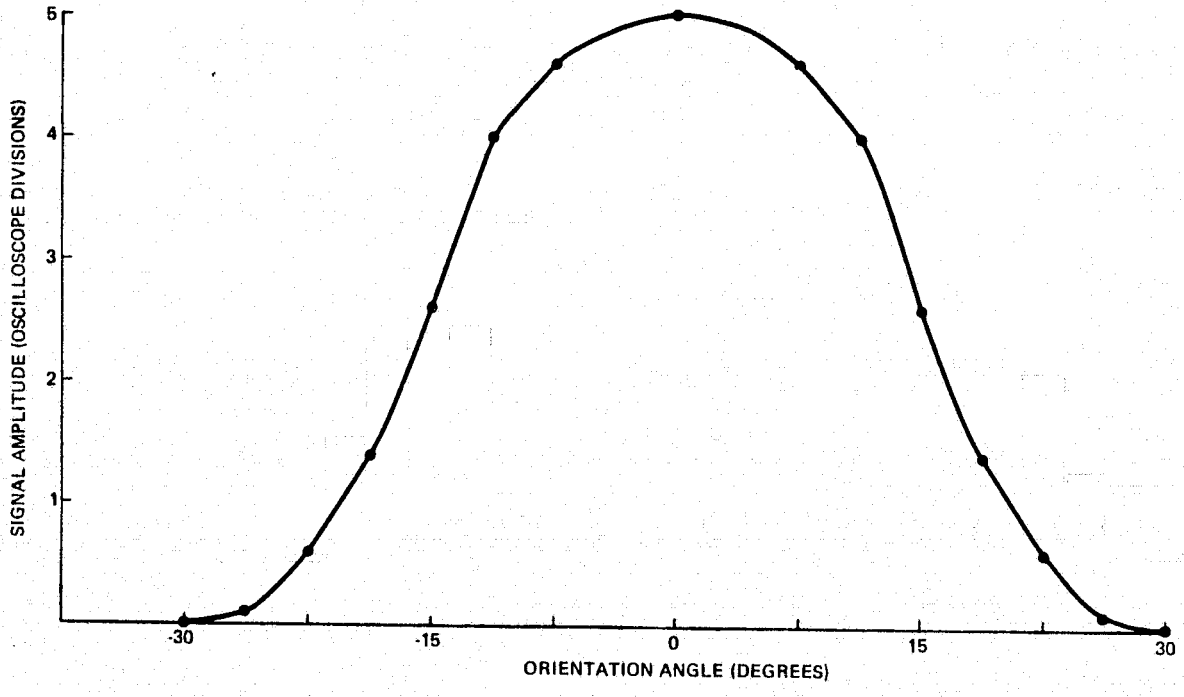

Figure 16. Return Pulse Amplitude as a Function of Rotation Angle

If the construction of the individual retroreflectors in Figure 9 is examined closely it will be noticed that each element is enclosed in a protective metal cover or can which serves two purposes. According to the vendor the two purposes are to keep dust from settling on the mirror surfaces and to protect the sharp edges of the retroreflector mirrors from accidental damage and/or the operator from accidental injury. In the initial cursory examination of the units it did not appear that the covers formed a significant limit to the field-of-view performance. The measured field-of-view performance, however, was not adequate and hence a further check of the effect of the cover restriction was made. Figure 17 is a plot of the return pulse amplitude as a function of relative rotation angle for a retroreflector whose metal cover had been cut back in order not to obstruct any portion of the retroreflector. The two curves shown in Figure 17 are for rotation of the retroreflector about two orthogonal axes. The measured field-of-view of approximately 65° between the 10% amplitude points is far superior to the 45° field-of-view of the standard, partly covered, unit.

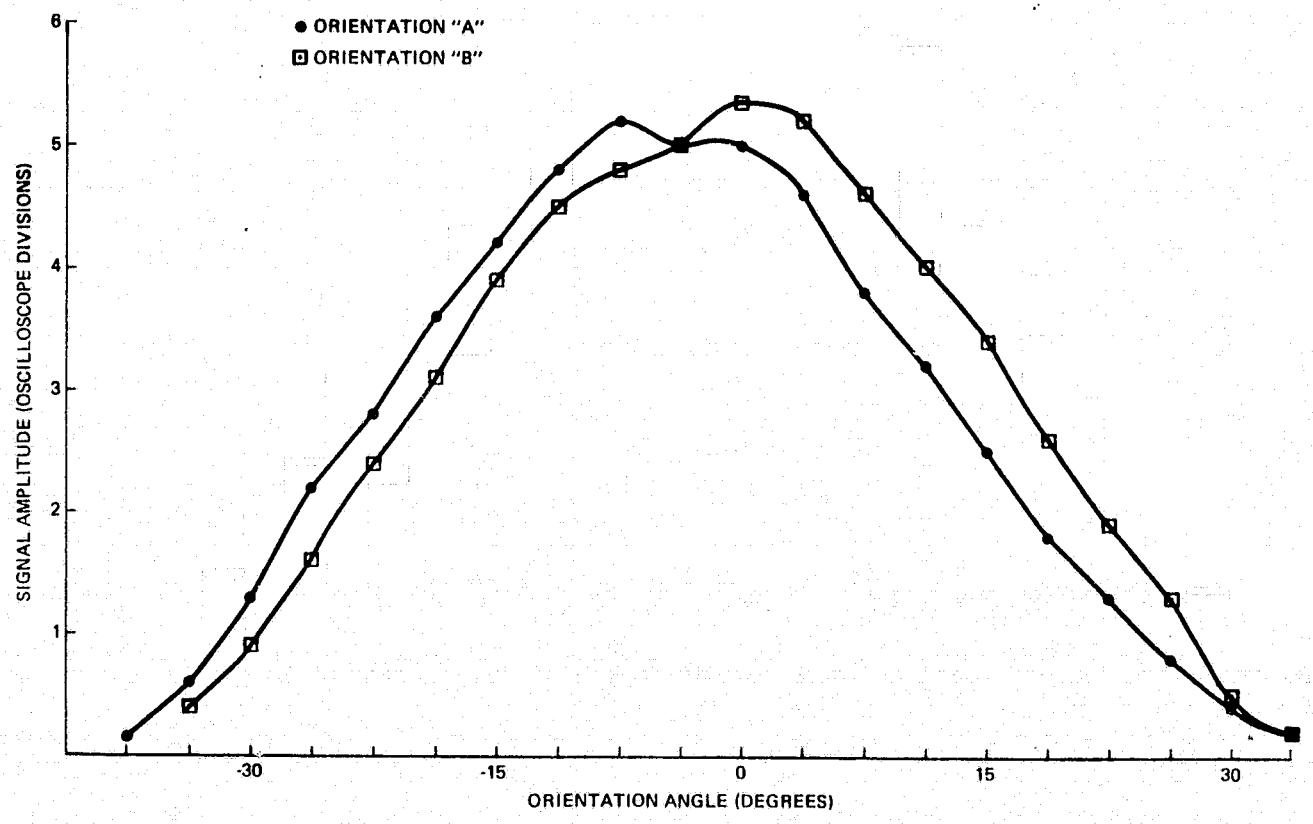

Figure 17. Return Pulse Amplitude as a Function of Rotation Angle for Retroreflector with Cover Removed

In a further investigation of the angular response of the retroreflectors, the display amplitude plot of Figure 17 was converted to the relative power plot of Figure 18. The conversion from oscilloscope amplitude to relative power was made with the aid of the curve fitting data calibration discussed in Section 4.2. The relative power curve of Figure 18 was then compared with the theoretical angular response curves plotted by other authors*. A plot of the predicted relative response for a retroreflector with square sides is given in Figure 19. The predicted response of Figure 19 agrees with the data of Figure 18 within approximately 20% which is well within experimental error.

Also plotted in Figure 19 is the relative response of a retroreflector with triangular sides having the same side dimensions as the square-side unit. Although the triangular-side device response is smoother and decreases in amplitude more slowly, the square-side retroreflector returns more signal for all orientations. The triangular side device was originally selected and studied for its uniform response, however, the square side device was ultimately selected for its increased return signal characteristic.

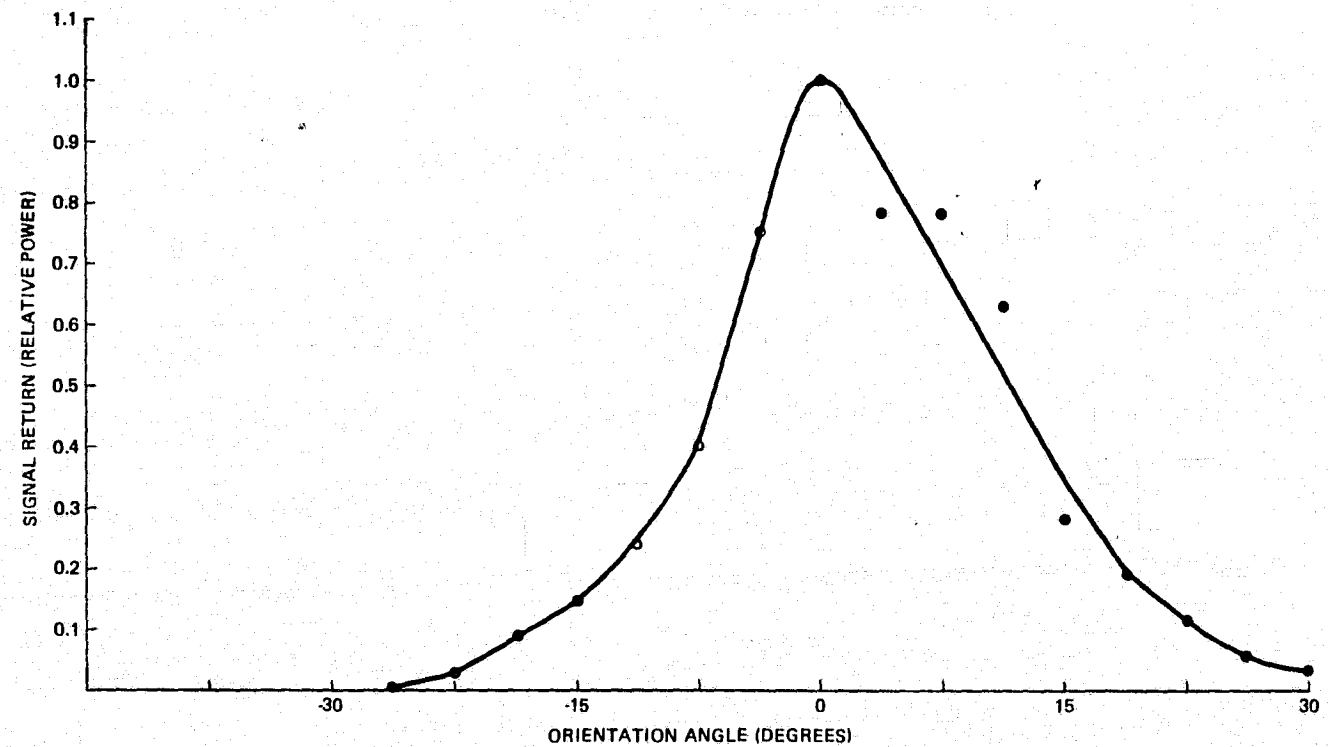

Figure 18. Retroreflector Relative Power Response

*RCA Electro-Optics handbook EOH-11 pp 217-224.

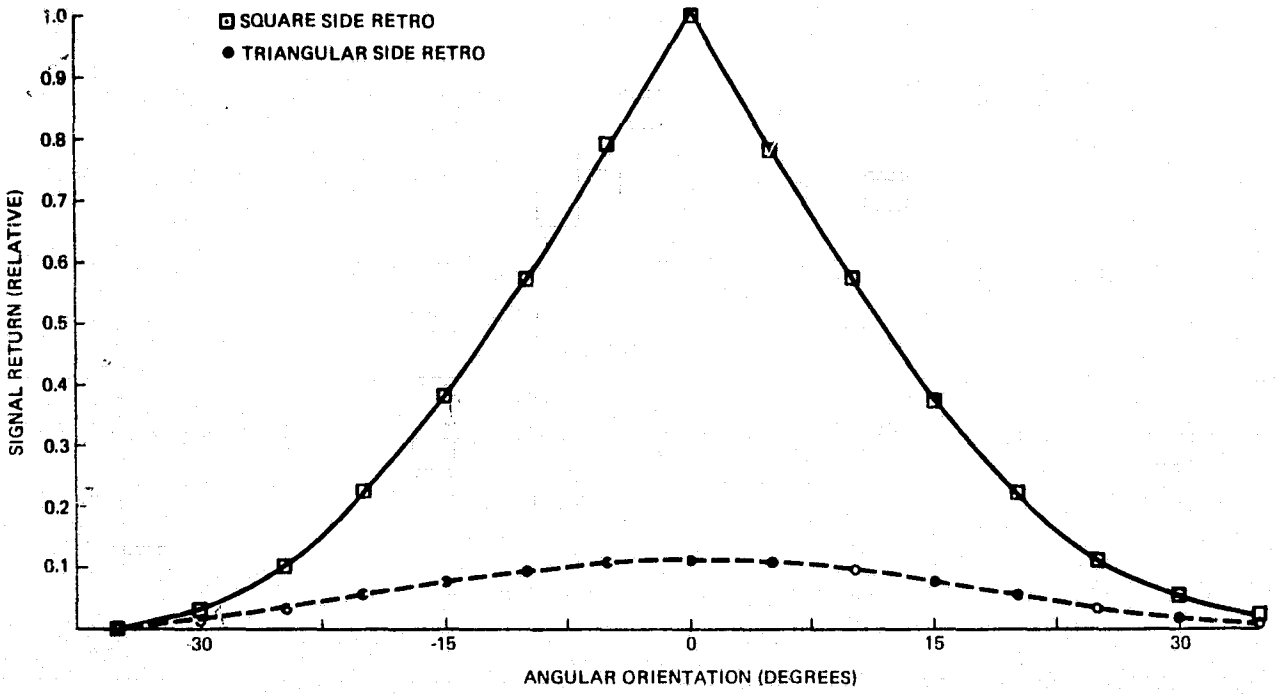

Figure 19. Predicted Retroreflector Relative Response

The measurements of a non-covered retroreflector unit demonstrated superior performance and, therefore, the same cover removal process was performed on all of the units on the satellite mock-up. A photograph of the modified units installed on the satellite mock-up appears in Figure 20. The resulting wider field-of-view appeared to give adequate results for the final series of tests as described in Section 4.7.

4.6 Range Considerations

In addition to the interaction with the retroreflectors on the satellite mock-up, the ladar signal return is also influenced by a number of factors having to do with the optical range. The length of the 695 m (2280 ft) range leads to a constant attenuation factor in the computation of the range equation. Additional attenuation parameters include absorption of the beam because of water vapor and various other gases in the range path, as well as distortions in the return beam because of turbulence and/or heat waves. The latter can have beam steering effects which cause the transmitted beam and/or return signal to wander. Also, the index of refraction gradients cause distortions in the

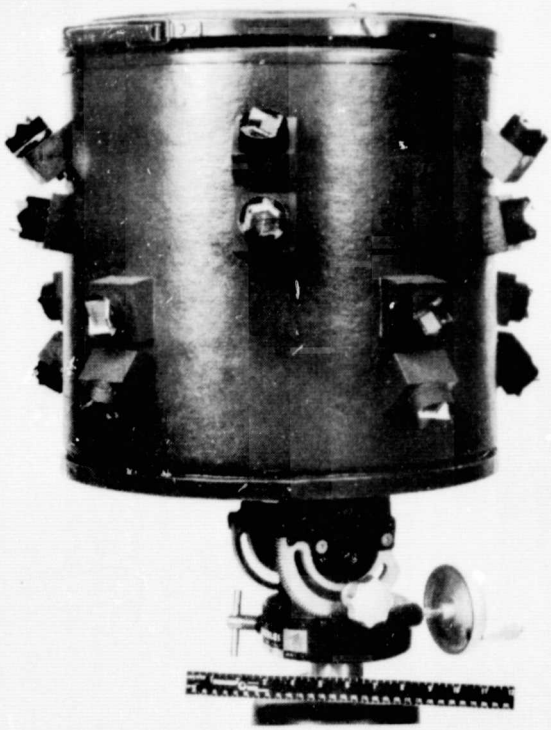

Figure 20. Modified Retroreflectors Installed on Satellite Mock-up

return signal wavefront which can significantly reduce the effective heterodyne efficiency with the uniphase LO laser beam. A vivid illustration of these distortions, as seen through a high power telescope, may be seen in the videotape presentation delivered as a part of this report (Appendix D). The mirage type effects are visible in many sections of the tape which show the satellite mock-up location at the range tower.

Another potential range problem, which was discovered in viewing the videotape recordings of the telescope viewed range path, was that trees and/or brush could possibly block the retroreflectors. It was found that some branches which were normally not a problem could be blown over into the range path for brief periods during strong gusts of wind which occurred on some range test days. The condition is visible on some of the videotape sequences. To eliminate the problem a number of small trees and/or limbs were cut down prior to the final satellite survey tests and the mock-up was located at a higher elevation.

4.7 Final Satellite Survey

Upon completion of the various studies discussed in the previous sections, a final survey of the satellite mock-up with the Norden breadboard ladar system was made. A videotape delivered as Appendix D of this report contains segments of the data as it was taken. For most of the survey data the mock-up was placed on the end of a boom and extended out and down from a platform on the range tower. Photographs of the boom suspended condition appear in Figures 21 and 22. The satellite mock-up was slowly rotated by means of a Tee handle on the platform end of the boom. One segment of the videotape data shows the actual rotation of the mock-up as seen through the high power telescope from the ladar transceiver location. Another segment of the videotape shows the signal return from the target as it was rotated with the beam scanning stopped. A real time scanning display with the rotating satellite mock-up and a stationary reference retroreflector mounted on the tower wall is shown in another segment of the videotape. Figure 23 is a direct photograph (not videotape) of the raster scan which shows the satellite retroreflector return (upper dot) and the wall retroreflector return (lower dot).

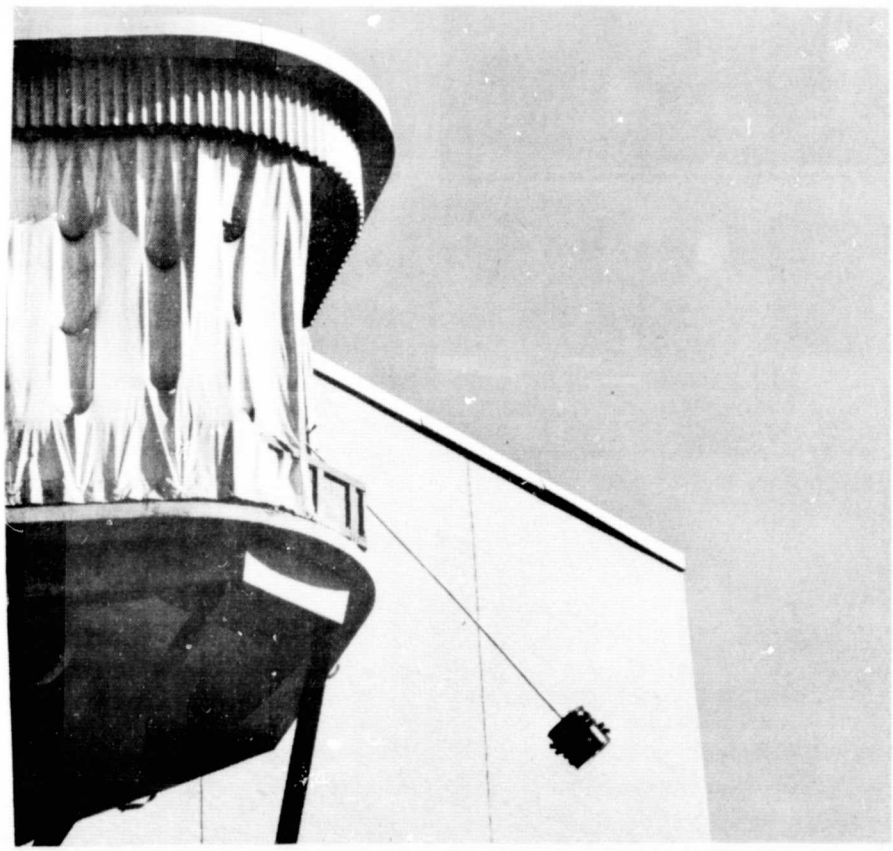

Figure 21. Boom Suspended Satellite Mock-up

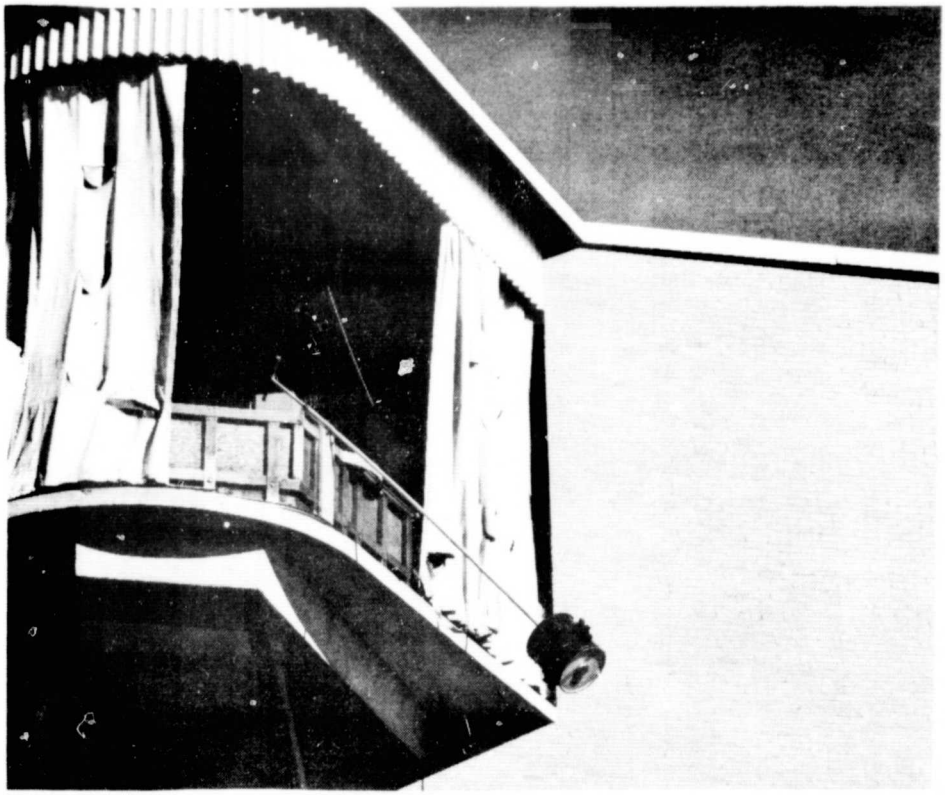

Figure 22. Alternate View of Boom Suspended Satellite Mock-up

The non-scanning signal return from the rotating target can be used in conjunction with the amplitude response scale described in the calibration measurements section to determine the maximum-to-minimum signal return ratio and to examine the coherent sum and difference effects for the final (cover removed) retroreflectors. The data shows that the average signal return does not decrease to zero as was the case originally when the retroreflectors had the protective covers. The coherent sum and difference effects only produce a complete zero over a narrow range of rotation angles; the rapid variation from sum to difference in this angular region is of course caused by the beam steering effects of the turbulent atmosphere -- which would not be present in extraterrestrial applications.

The videotape data of the scanning display is a recording in real time of a single raster frame, such as shown in Figure 23. The videotape allows the examination of the data from many frames by observers from various viewpoints -- on a frame-by-frame basis, if necessary. One videotape segment displays the scan pattern where return data is processed with a maximum signal-to-noise ratio of approximately 30-40 dB. Under these conditions there did not appear to be any drop out of the return signal during

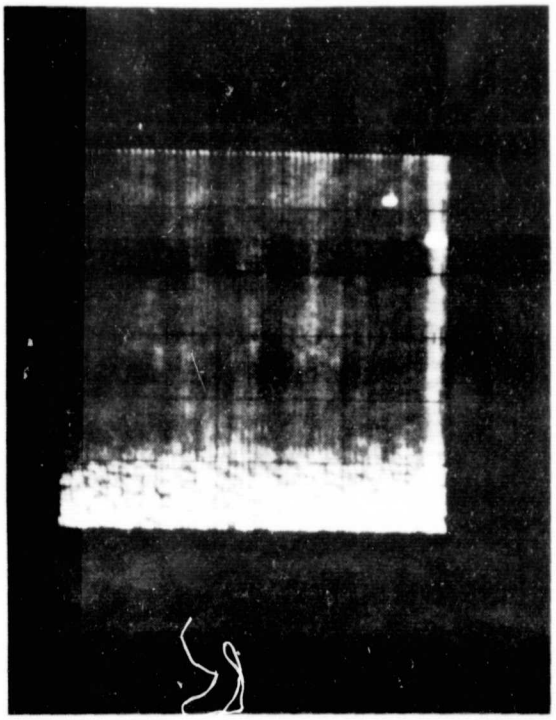

Figure 23. Direct Photograph of Raster Scan Ladar Display

20 scans of the target. When the signal-to-noise ratio was decreased to approximately 15-18 dB, there were a number of noticeably weaker returns which indicated reduced or missing returns during some of the 16-20 hits expected during each scan of the target.

Scan data was also taken for the maximum (30-40 dB) and 15-18 dB signal-to-noise ratios with satellite rotation stopped at a location corresponding to a worst case condition relative to the coherent sum and difference effect. Here the data also had no discernible drop outs of return signal for the maximum case and about three out of thirty two scans were lost for the 15-18 dB case.

4.8 SUMMARY

During the course of the study of the ladar response to a satellite mock-up, a great many experimental investigations and observations were made. Among the more significant items were the following:

a. Detection of a rotating satellite mock-up by a 10.6 μm ladar over an outdoor range of 695 m was demonstrated.

b. The icosahedron retroreflector array was found to provide a non-zero average signal return for all measured attitudes of the satellite.

c. The angular response of the retroreflectors was measured.

d. Coherent sum and difference effects between adjacent retroreflectors were identified and investigated. The effects will have to be taken into account in the configuration design.

e. Atmospheric beam steering and distortion effects were identified.

f. Real time and integrated raster scan and other selected display returns of target as well as telescope object data recording techniques were employed.

APPENDIX A
SCAN OPTIMIZATION

A.1 Summary

Reference is made to the four-line scan described in Report No. 1247 R 0004, paragraph 5.2.2.2.3. The probability of detection per frame was obtained for a point target, as a function of the degree of beam overlap and of the phase angle of the scan mirror at the occurence of a laser pulse. The results confirm that the optiumum phase angle is 18° 26', and document a trade-off between PRF and peak pulse power by the variation of the scan scale. The plotted results show the sensitivity of the probability of detection to phase angle error, and indicate the optimum scan scale factor.

A.2 Description of the Four Line Scan

The scan, illustrated in Figure A-1, is performed in elevation by a mirror oscillating at one-fourth of the PRF. One laser pulse occurs when the mirror is at a phase ϕ= 18° 26 of its sinusoidal oscillation; the subsequent pulses are delayed by multiples of 90°. The resulting elevation scan consits of four equally spaced lines, and can be represented by:

$$\theta_j = A \sin (18°26' + j \times 90°)$$

where

j is the pulse number
A is the amplitude of the sinusoidal scan.

Let A=1; for the case described in 1247 R 0004, the peak of one beam is at the -3 dB point of the adjacent beam. The line spacing $\Delta\theta$ is approximately given by $\Delta\theta$= sin (18°26'+90°) -sin 18°26' = 0.633.

A.3 Power

The normalized power corresponding to a target of elevation θ and a beam of elevation θ_j is expressed by

$$P(\theta, j) = e^{-a(\theta-\theta_j)^2},$$

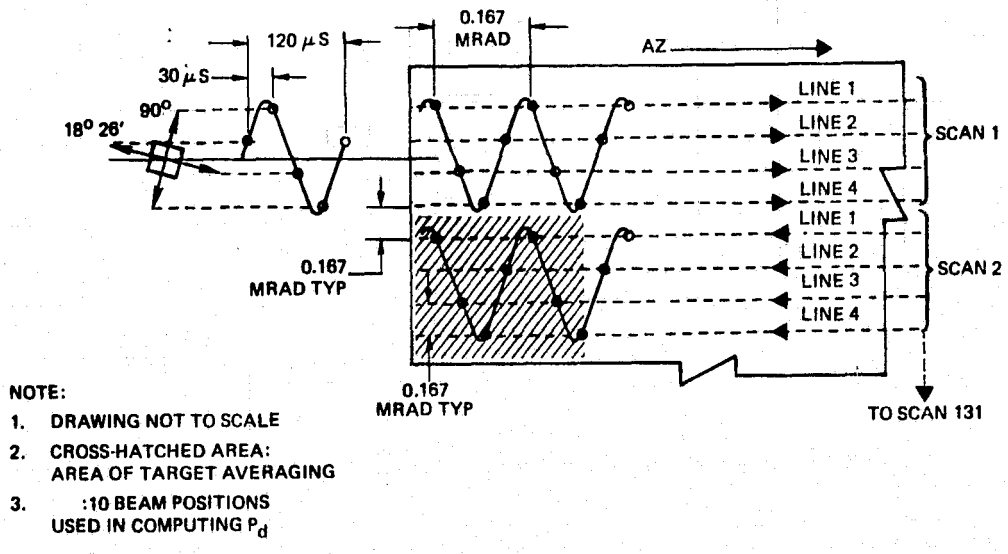

Figure A-1. Four-Line Scan (ϕ = 18°26')

where

α is given by the solution of

$$e^{-\alpha(\Delta\theta)^2} = 0.5$$

or

$$\alpha = 1.74.$$

If, in addition, the target and the beam are separated by the azimuth difference $(\phi-\phi_j)$, then

$$P(\theta,\phi,j) = e^{-\alpha[(\theta-\theta_j)^2+(\phi-\phi_j)^2]}.$$

A.4 Probability of Detection

The recieved waveform can consist of noise only, or of a target echo plus noise. The criterion used to decide that a target is present, is the fact that the received signal envelope exceeds a predetermined threshold voltage.

For the case of a narrow-band signal, and of white Gaussian noise, the probability of detection is given by the function*

$$Q(a,b) = \int_b^\infty x e^{-(x^2+a^2)} I_o(ax)\,dx$$

where

$a = \sqrt{2\ S/N}$, a function of the signal-to-noise-ratio

b is a number related to the probability of false alarm, Q_o, by the relation:

$$b = \sqrt{-2 \ell n Q_o}$$

$I_o(ax)$ is the modified Bessel function.

The Q function is evaluated by the use of the approximation*

$$Q \cong \text{erfc}\ \left(\frac{b-a}{\sqrt{2}}\right) + 2a^{-1} \cdot (2\P)^{-\frac{1}{2}}$$

$$\cdot \left[1 - \frac{b-a}{4a} + \frac{1+(b-a)^2}{8a^2}\right] \cdot \exp\left[-\frac{1}{2}(b-a)^2\right],$$

which was found to be quite accurate for the range of a and b used in the computations,

A.5 Effective Probability of Detection

A compound probability of detecting a target in one scan frame, P, is defined by taking into account the individual probabilities, p_i, of detecting the target on any of N neighboring laser beams:

$$P = 1 - \prod_{i=1}^{N} (1-p_i).$$

---

*C. W. Helstrom, Statistical Theory of Signal Detection, Pergamon press, 1968; pp 166-171, and Appendix F.

*OP. cit. Appendix F; equation F.15 which contains three errors is corrected in the expression for Q.

An effective probability of detection, per scan frame, is defined by averaging P over all possible positions of a target relative to the scan raster. Because of the periodicity and symmetry of the scan, the averaging is performed over a limited area. Under the assumption that the target is equally likely to occur in any position, the averaging was performed over a rectangular array of 7x13 points, matching the cross-hatched area of Figure A-1.

A.6 Scale Factor and PRF Versus Peak Power Trade-Off

A scale factor, k , was introduced to permit varying the spacing of adjacent beam from the value referred to in Section A-2, where the peak of one beam falls on the -3 dB point of the adjacent beam.

Since the scale change affects both the beam raster (index j) and the target raster used in the averaging process (index i), the signal power can be expressed as:

$$P_{i,j} = e^{-\alpha k^2 [\theta_i - \theta_j)^2 + (\phi_i - \phi_j)^2]} .$$

The number of laser pulses required to cover a scan frame is reduced by the factor k. If the frame time is maintained constant, then the PRF can be reduced by the same factor, and it is assumed that this reduction can be accompanied by a similar increase in the peak pulse power. Under that assumption the signal power is finally expressed as

$$P_{i,j}(k) = k^2 e^{-\alpha k^2 [(\theta_i - \theta_j)^2 + (\phi_i - \phi_j)^2]} .$$

A.7 Signal-to-Noise Ratio

The signal-to-noise ratio, used to determine the parameter a of the Q function, is defined on the basis of an arbitrary value of the S/N for the nominal case, k = 1:

$$\left[\frac{S}{N}\right]_{peak}(k) = \frac{P_{peak}(k)}{P_{peak}(1)} \cdot \frac{S}{N} = k^2 \cdot \frac{S}{N} .$$

Thus

$$a_{peak}(k) = \sqrt{2\left[\frac{S}{N}\right]_{peak}}(k) = k\sqrt{2\frac{S}{N}}$$

$$= \sqrt{2}\, k \exp[0.05 \ell n 10 \times (\frac{S}{N} \text{ in dB})],$$

and, for the general case where the target is not on the beam axis ($\theta \neq \theta_j, \phi \neq \phi_j$):

$$a_{i,j}(k) = a_{peak}\sqrt{\frac{P_{i,j}(k)}{P_{peak}(k)}} = a_{peak}(k) \times \frac{1}{k}\sqrt{P_{i,j}(k)}$$

$$= \sqrt{2} \exp[0.05 \ell n 10 (\frac{S}{N} \text{ in dB}]\sqrt{P_{i,j}(k)}.$$

A.8 Probability of False Alarm

In the standard scan (k=1), a probability of false alarm, per doppler channel, per pulse, $P_{fa} = 10^{-7}$ is used (Report 1247 R 0004, page 4-13). The total number of false alarms per scan frame, N, equals

$$N = P_{fa} PRF_{\tau}$$

where τ is the frame period.
In the trade-off, N and τ are kept constant, while the PRF is divided by the factor k^2. Thus

$$P_{fa}(k) = P_{fa}(1) \times \frac{PRF(1)}{PRF(k)} = k^2 \times 10^{-7}.$$

This leads to the following value for the parameter b of the Q function:

$$b = \sqrt{-2 \ell n (k^2 \times 10^{-7})}.$$

A.9 Results

The effective probability of detection was computed (Figure A-7) for two nominal values of signal-to-noise ratio; i.e., 8 dB and 12 dB. In each case the scale factor k was allowed to vary while the phase angle ϕ was maintained constant, and vice versa. The resulting sections of the surface $P_{effective}(k,\phi)$ are plotted in Figures A-2 through A-6.

The following statements can be made:

a. The curves are symmetric with respect to ϕ=o.

b. The maximum for any given value of k seems to occur in the vicinity of ϕ=18°26', as expected.

c. The optimum value of k is in the vicinity of 2.4, and corresponds to a PRF of $\frac{33,333\text{Hz}}{(2.4)^2}$ = 5787 Hz and a beam overlap at the k^2x-3 dB = -14.4 dB point; the lowest power response, for a target midway between adjacent beams, is -3.6 dB.

d. The performance is not very sensitive to variations in the phase angle, ϕ.

An effective power loss is evaluated from the a argument corresponding to the value of Q equal to P_{eff}. The inversion of the Q function was accomplished by consulting the Rand Table of Q functions*. The resulting curve, derived from the data of Figure A-2 (k=2.4) is plotted in Figure A-6; it shows zero sensitivity in the vicinity of ϕ=o, 18° 26' and 45", and a maximum sensitivity of 0.08 dB per degree of phase in the vicinity of ϕ=30°. The wost effective power loss, 1.4 dB, with respect to $\phi_{optimum}$= 18° 26', occurs at ϕ=45°.

---

* J. I. Marcum, Table of Q Functions, 1 Jan. 1950, ASTIA AD116551

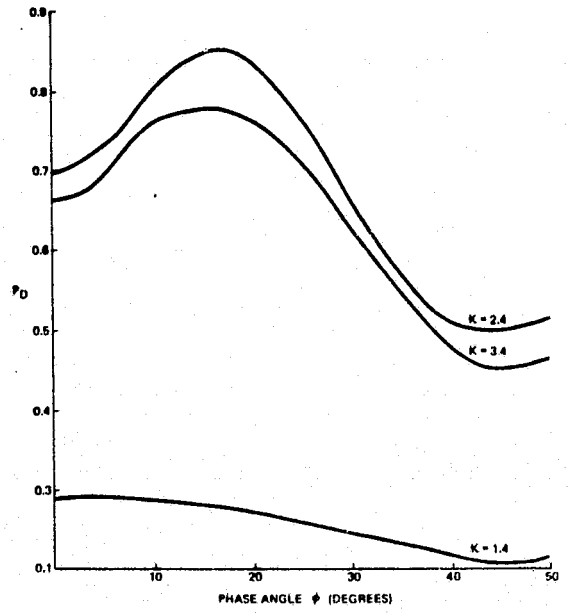

Figure A-2: Probability of Detection Versus ϕ for S/N at Peak of Reference Beam = 8 dB

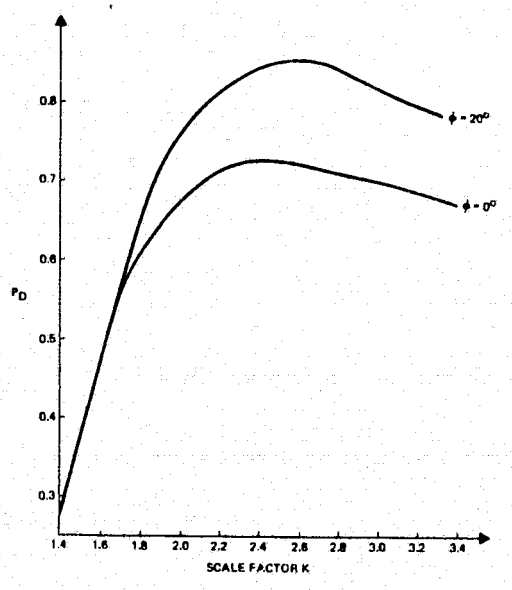

Figure A-3: Probability of Detection Versus k for S/N at Peak of Reference Beam = 8 dB

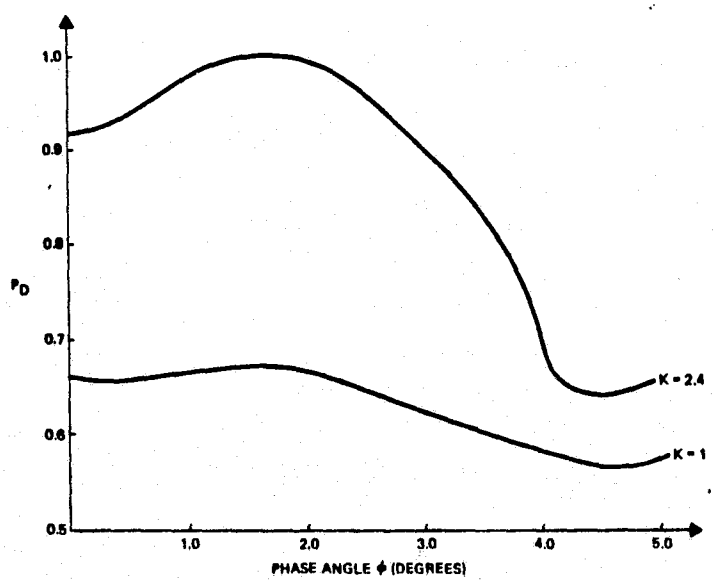

Figure A-4: Probability of Detection Versus ϕ for S/N at Peak of Reference Beam = 12 dB

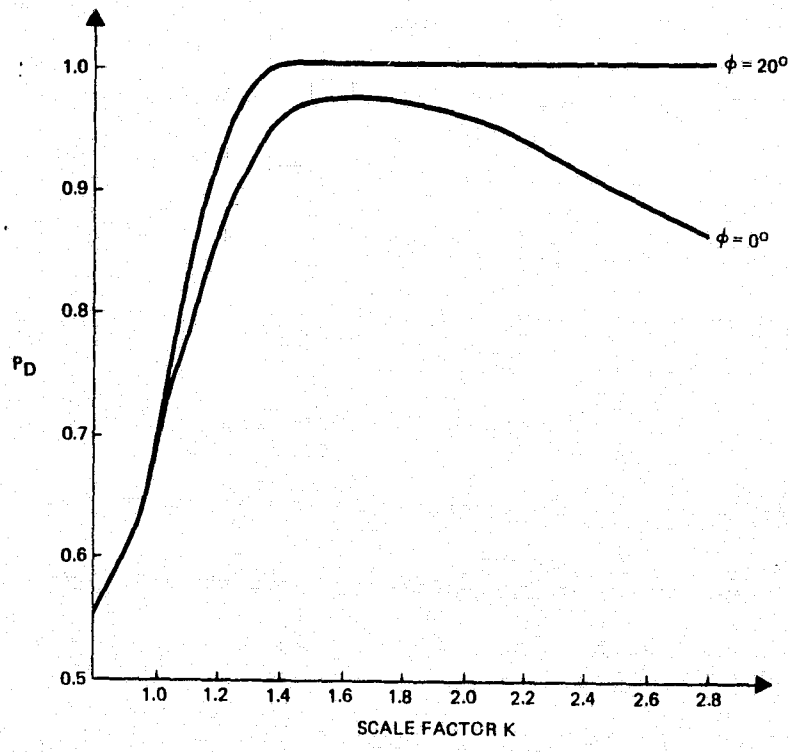

Figure A-5: Probability of Detection Versus k for S/N at Peak of Reference Beam = 12 dB

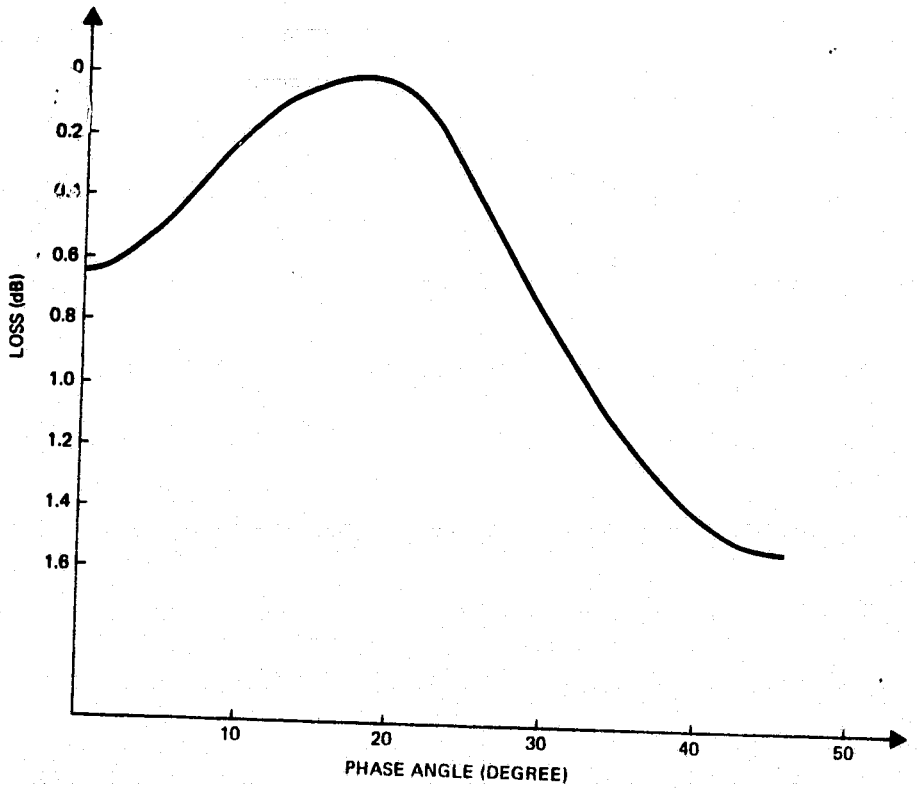

Figure A-6 Effective Power Loss Versus Phase Angle (Referred to Optimum Phase Angle)

```
00100 ?SCAN OPTIMIZATION VS SCALE FACTOR AND PHASE ANGLE
00110 J=.316
00120 DEF FNQ(A,B): GOSUB 00730
00130 PRINT "DB=";
00140 INPUT D7     ?S/N(DB) AT PEAK OF BEAM FOR K=1
00150 J1=.3333333  ? LATTICE CONSTANT FOR TARGET DISTRIBUTION
00160 PRINT "K=";
00170 INPUT K      ?LINEAR SCALE FACTOR FOR SCAN FRAME AND J1
00180 K2=K*K
00190 A8=1.414*EXP(.115129*D7)
00200 B=SQRT(-2*LOG(1E-7*K2))
00210 PRINT "PHI=";
00220 INPUT E4     ? PHASE ANGLE (DEGREES)
00230 S=0
00240 V=5.0132565
00250  A1=.278393
00260  A2=.230389
00270  A3=.000972
00280  A4=.078108
00290 P=PI/180
00300 E1=E4*P
00310 FOR M=1 TO 8      ? SET UP SCAN
00320 M1=M-5
00330 X(M)=(M1+.5)*.09029
00340 Y(M)=SIN(E1+M1*1.5701)
00350 W(M)=Y(M)
00360 NEXT M
00370 B1=0              ? FIND Y MIN
00380 FOR I=1 TO 3
00390 IF Y(I)<=Y(I+1) THEN 00440
00400 B1=1
00410 A=Y(I+1)
00420 Y(I+1)=Y(I)
00430 Y(I)=A
00440 NEXT I
00450 IF B1=1 THEN 00370
00460 FOR I=1 TO 4     ? IDENTIFY I FOR Y MIN
00470 IF W(I)=Y(1) THEN 00490
00480 NEXT I
00490 X(9)=X(I)
00500 X(10)=X(I+4)
00510 FOR I=1 TO 8
00520 Y(I)=W(I)
00530 NEXT I
00540 Y(9),Y(10)=W(I)+2.52
00550 N=0    ? COMPUTE AVERAGE PROBABILITY
00560 FOR X2=-J TO J STEP J1*J
00570 FOR Y2=0 TO 4*J STEP J1*J
00580 N=N+1
00590 H=1
00600 FOR M=1 TO 10
00610 P(M)=K2*EXP(-K2*1.735366*((X2-X(M))↑2+(Y2-Y(M))↑2))
00620 A=A8*SQRT(P(M))
00630 H=H*(1-FNQ(A,B))
00640 NEXT M
00650 S=S+1-H
00660 NEXT Y2,X2
00670 S=S/N
00680 PRINT
00690 PRINT "PROBAB. OF DETECT.=";S
00700 PRINT
00710 PRINT
00720 GOTO 00130
00730 IF A<1 THEN 00840? Q-FUNCTION SUBROUTINE
00740 C9=B-A
00750 D9=C9*C9
00760 X9=C9*.70711
00770 IF X9>=0 THEN 00810
00780 X9=ABS(X9)
00790  E=2-1/((((A4*X9+A3)*X9+A2)*X9+A1)*X9+1)↑4
00800 GOTO 00820
00810  E=  1/((((A4*X9+A3)*X9+A2)*X9+A1)*X9+1)↑4
00820  Q=.5*E*EXP(-.5*D9)*(1-C9/(4*A)+(1+D9)/(8*A*A))/(A*V)
00830 RETURN Q
00840 Q=0
00850 RETURN Q
```

Figure A-7. Computer Program Listing (Superbasic)

APPENDIX B
RANGE AMBIGUITY RESOLUTION BY LASER PRF JITTER

B.1 Summary

The passively Q-switched CO_2 laser was observed to exhibit a pulse-to-pulse interval jitter within a control loop stabilizing against long term PRF drifts. This jitter is utilized in a method which determines the unambiguous range to a target by matching echo receiving times with a set of recorded pulse transmitting times.

B.2 Observation of Pulse Repetition Interval (PRI) Jitter

The PRF-stabilized laser pulses were allowed to illuminate a detector whose output was viewed on a cathode ray oscilloscope. The sweep was triggered by the signal itself, and a jitter was observed in the position of the first pulse following the trigger pulse. The jitter was crudely estimated at ±2 μs, corresponding to ±1σ, for an average PRI of 44 μs.

It was hypothesized that the jitter, or departure from the average pulse position, is independent from pulse to pulse. To test the hypothesis the source signal was displayed on the scope using a sweep delayed by a variable time, which allowed the observation of the n^{th} pulse following the trigger pulse, for all values of n from 1 to 45. The readings are tabulated below.

n	Estimate of σ_n (μs)
1	2.0
3	3.0
7	3.5
12	4.0
16	6.0
20	6.5
30	8.0
40	10.
45	10.

For completely correlated varations in PRI, the expected functional dependence of σ_n on n is $\sigma_n = n\sigma_1$, and for completely independent variations it is $\sigma_n = \sqrt{n}\,\sigma_1$. The tabulated readings have the approximate form $\sigma_n = \sqrt{n}\,\sigma_1$ which confirms the hypothesis.

B.3 Ranging Design

A precise clock is used to time the transmission of each ladar pulse, and a timing record is kept for a number N of pulses corresponding to the round-trip time to the farthest expected target position

$$N = \frac{2R}{c\tau}$$

where R is the range (m)

c, the speed of light (ms)

τ, the pulse period (s)

Thus two illustrative cases, with τ = 50 μs, yield N = 7 and N = 134 for target ranges of 50 and 1000 Km, respectively. Similarly, a running record is also kept of the times of the latest m received echo pulses, the value of m to be determined in this analysis.

The m time records are then matched with various sequences of m consecutive transmit times corresponding to the expected range uncertainty. Each match is performed by shifting all transmit times to bring the initial pulse times of the transmit and receive sets into coincidence. A matching criterior is then evaluated, which is the RMS of the time differences of corresponding pulses in the two sets. A match is declared when the criterion falls below a predetermined threshold. The time shift which produces a match is the signal round-trip time and it determines the target range.

B.4 Analysis

The independence of consecutive pulse intervals facilitates the analysis of the ranging design. Let the timing uncertainty because of the finite clock period be designated by σ_o.

For the set of two sequences to be matched, each consisting of N pulses, let the first pulses of each sequence be brought into coincidence by a time shift of one sequence.

A criterion K, measuring the goodness of the match can be defined as follows:

$$K \triangleq \frac{1}{N-1}\left[\sum_{j=2}^{N} (t_{1_j} - t_{2_j})^2\right]$$

Two cases exist.

1. The sequences are matched.

   In the presence of a small noise background K has an upper bound of $2\sigma_o^2$.

2. The sequences are mismatched.

   Here the expected value of K is

$$\bar{K} = \frac{1}{N-1}\left[\sum_{j=2}^{N} (2\sigma_j^2)\right]$$

$$= \frac{1}{N-1}\left[\sum_{j=2}^{N} 2j\sigma_1^2\right] = \sigma_1^2 \frac{(N+2)(N-1)}{(N-1)}$$

$$= \sigma_1^2 (N+2).$$

Let a statistic Q be defined $Q = \dfrac{\frac{1}{N-1}\left[\Sigma(t_{1_j} - t_{2_j})\right]}{2\sigma_o^2}$

where expected value: $\bar{Q} = \dfrac{\sigma_1^2 (N+2)}{2\sigma_o^2}$

A threshold ,T, can now be set, such that if Q<T a match can be declared with a desired probability of false match, and a specified probability of rejecting an existing match.

Reference is made to the Statistics Manual, E.L. Crow, F.A. Davis, M.W. Maxfield, Dover Publications pp. 76-77, and Chart VIII, where λ is equivalent to $\sqrt{Q}$.

Determination of N (sample size)

In the case of a match Q = 1. If $\sigma_1^2 = k\,\sigma_o^2$, then, in the case of a mismatch $\bar{Q} = \dfrac{k\ (N+2)}{2}$, corresponding in the

reference to a value of $\lambda = \frac{\sqrt{k\ (N+2)}}{2}$. Chart VIII permits a trade-off between the number of pulses N = n + 1 to be matched and k. For a given value of β, the probability of accepting a match where there is none (false alarm) can be determined. Thus for a probability of detecting a match, $\alpha = 0.95$, and a false match $\beta = 0.05$, it is found that for k = 1 it is sufficient to process a sequence of 8 pulses.

Appropriate decision thresholds can be found in Table 5 of the cited reference.

B.5 Conclusion

From this preliminary analysis it is evident that the number of pulse operation intervals to be matched is small and will not place an undue burden on the system computer. Any reasonable probability of detecting a match and probability of falsely detecting a match can be implemented by suitable values of k and N.

APPENDIX C
MAGNETIC TRANSDUCER

C.1 Introduction

A wideband response is needed in the laser control loop which locks the two lasers together and controls the PRF. The loop bandwidth is actually limited by two factors. One is the resonance in the PZT transducers which results from the cantilever design of stacked crystals. The second is the nature of the discriminator which is used to compare the laser frequencies and control the IF frequency. The discriminator problem stems from the fact that the phase comparison must be made in a few cycles of the carrier; i.e., a very wide band discriminator is required and a hold circuit is necessary in order to ensure that the error value is used in an optimum fashion.

The problem of the resonances in the PZT transducers is more basic. Measurements have indicated that the particular devices being used have a resonance at 2200 Hz with a Q of about 6. Compensation is accomplished by making open-loop response measurements and using some sort of viscous material to support the structure. Alternately, the problem can be solved by replacing the PZT transducers with devices which are inherently overdamped. Accordingly, a magnetically excited device with a readily controlled damping ratio has been conceived to achieve the required deflection and accuracy.

C.2 Background and System Requirements

The use of PZT transducers is a well established technology. The devices are useful primarily because they offer a very low mechanical hysteresis in the lateral direction. The traditional technique for modulating the length of a laser cavity involves fastening the laser mirror to a linear PZT transducer or a series stack of such transducers. In the NASA rendezvous sensor configuration, both the pulsed laser transmitter and the continuous wave local oscillator had been tuned in this fashion.

Historically, PZT transducers were selected for short wavelength optical systems because a hysteresis-free linear motion was required only over a very small range. When longer wavelength lasers appeared, greater linear motion was required. Since the PZT devices were already developed, it was relatively simple to construct a compound transducer from a number of individual devices connected mechanically in series and electrically

in parallel. However, since current system requirements require the lasers to be used in complex control loops, the drawbacks of the component PZT device are beginning to surface.

One of these drawbacks is the high PZT driving voltage and the associated driving circuit power losses. Another is the inherent mechanical instabilities caused by the stacking of several individual devices in order to achieve the required linear motion. The stacking results in an mechanically complex structure that is severely underdamped, causing inherent instabilities in the feedback loop.

C.3 Disadvantages of PZT Transducers

The rendezvous sensor PZT transducers have two drawbacks, as previously mentioned. The first is the high drive potential required and the consequent large driving circuit power drain. Current available devices required about 800 volts potential in order to achieve linear motion of less than one micrometer. One of the disadvantages in using this high a voltage is that the amplifiers dissipate close to ten watts per transducer, even through the transducers themselves do not dissipate any power. Thus, the amplifiers and associated power supplies are necessarily large and the conversion loss in the power supplies is also significant. Another disadvantage is that the control problem is more difficult because it is not feasible to utilize a push-pull output stage in the amplifiers. The transducers are driven in one direction only, causing nonlinearities to be introduced into the control loops.

The second drawback is that a stack of eight individual transducers is required in order to achieve the required onehalf wavelength of motion for a 10.6 micrometer laser. These transducers are glued together (mechanically in series) and operate electrically in parallel. The resulting electrically complex structure has a lightly damped resonance at 2700 Hz, making the closed-loop feedback system prone to instability with oscillations at or near 2700 Hz. The cantilever mechanical structure is also potentially sensitive to damage and instability from severe vibration.

When the required laser control loops are configured around the lightly damped PZT control devices, the critical control parameters are severely limited.

C.4 Experimental Program

As a part of the current effort, it was decided that the lack of an optimum transducer was a serious problem. Therefore, a magnetic transducer was designed and an initial breadboard was constructed. A photograph of the breadboard transducer is shown in Figure C-1.

The spring element in the breadboard was designed to be a simple circular structure, in order that various materials could be examined. The materials consisted of various rubber O-rings, and other silicone rubber products, with appropriate lubrication. Each of the spring materials tried had a common drawback - excess mechanical hysteresis. That is, the magnetic field deflected the surface but the surface did not restore to its original position when the magnetic force was removed. Since the large air gap in the design precludes magnetic hysteresis as the main cause, the mechanical properties of the spring are the dominant influence.

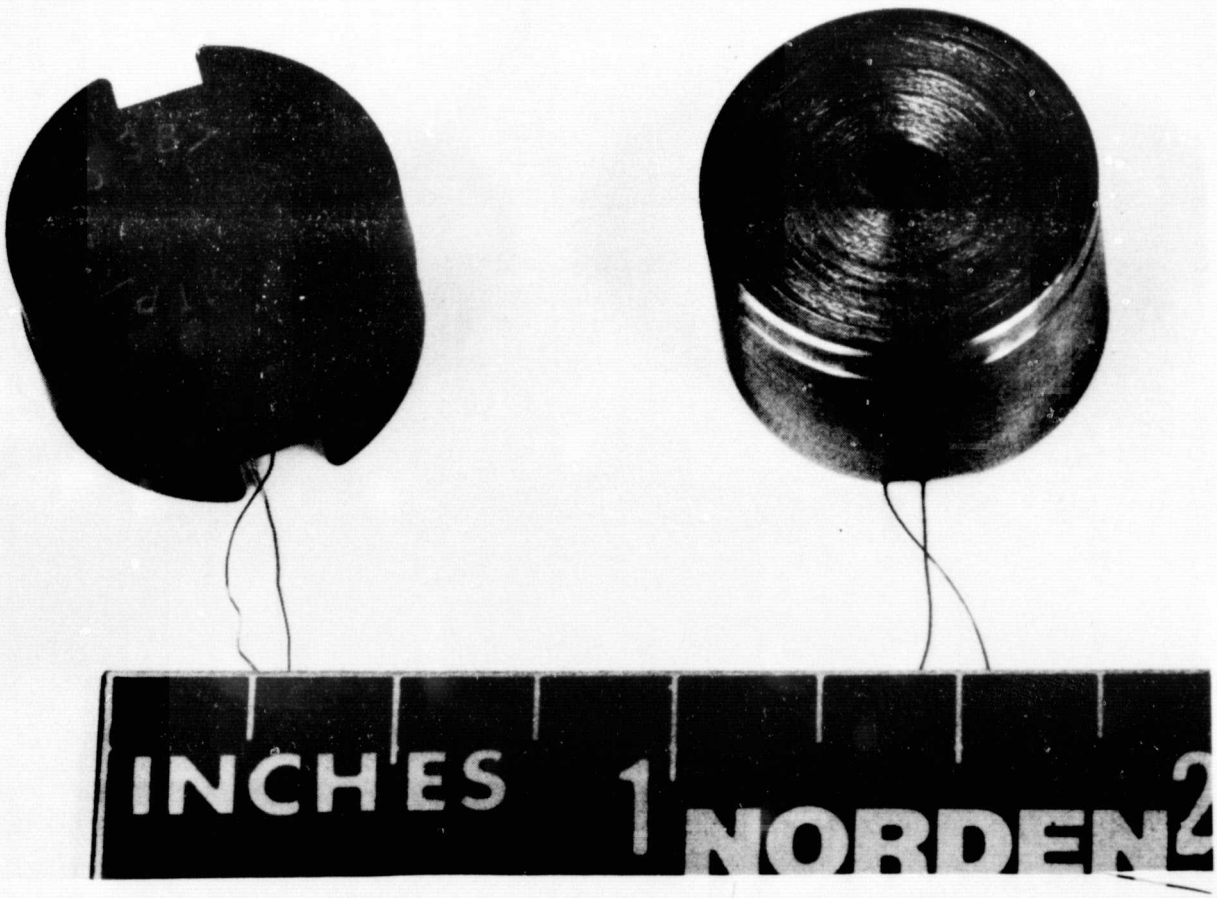

Figure C-1. Breadboard Magnetic Transducer

It is believed that the unit tested behaved satisfactorily in all aspects with the exception, however, of the choice of spring material. Therefore, the next task of the design effort was to locate a spring material with a minimum of mechanical hysteresis. Fortunately, such materials do exist; they are used in the construction of precision, spring restrained, rate gyroscopes. It is these alloys which were investigated for their applicability.

C.5 Design Effort

The fundamental design considerations for a magnetic driver are identical to the design criteria for a PZT driver. In order to tune the laser, the mirror must be capable of being positioned with the required accuracy. In addition, spurious motion must be kept to an absolute minimum. Mechanically, the device must be suitably compliant in the direction of motion while rigidly supported in the orthogonal axes. The mirror motion has six basic components, consisting of three translational components and three rotational components. The desired motion is in one translational axis only; the five remaining components can be expected to contribute to system errors.

C.5.1 Hysteresis

The required motion is one-half wavelength of 5.3 micrometers. The critical design parameter is the hysteresis, or inability of the spring material to return to its original position after it is deflected.

The required system stability is 100 kHz. The laser lines are at

$$\eta_k = k\frac{c}{2\ell}$$

where k is an integer. For a one meter cavity

$$\eta_k = k\frac{3\times10^8}{2} = 1.5\times10^8 k.$$

At 10.6 micrometers

$$\eta = \frac{c}{\lambda} = \frac{3\text{x}10^{8}}{10.6\text{x}10^{-6}} = 0.283\text{x}10^{14}$$

$$\therefore\ k = 1.89\text{x}10^{5}$$

Now:

$$\eta_k = \frac{1.89\text{x}10^{5}\text{x}3\text{x}10^{8}}{2\ell} = \frac{2.83\text{x}10^{13}}{\ell}$$

$$\frac{\delta\eta}{\delta\ell} = 2.83\text{x}10^{13} = \frac{\Delta\eta}{\Delta\ell}$$

for

$$\Delta\eta = 10^{5}$$

$$\Delta\ell = \frac{10^{5}}{2.83\text{x}10^{13}} = 3.53\text{x}10^{-9} \text{ meters} = 35.3 \text{ Angstroms } (\text{Å}).$$

C.5.2 Lateral Translation

Since the mirrors are flat in the present laser, lateral displacement of the mirrors has no effect. It is possible, however, that in the future a different resonator with curved mirrors will be used; e.g., a confocal resonator. For this case, a lateral displacement would have an effect proportional to the degree of curvature of the mirror. Since the mirror must move $\lambda/2$ or less, a lateral shift of 10% would be $\lambda/20°$. In a confocal laser resonator configuration the optical frequency and the PRF would be affected. However, since both parameters are controlled by a closed loop feedback system, the effects should be readily compensated with negligible effect on overall system operation. With ordinary manufacturing tolerances, orthogonal motion will readily be 5% or less of the displacement along the primary (Z) axis (see Figure C-2).

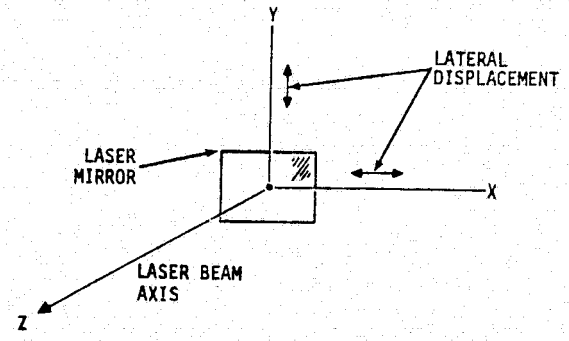

Figure C-2. Laser Beam and Mirror Coordinate System

C.5.3 Rotation About An Orthogonal Axis

Rotation of the mirrors about orthogonal axes (X, Y) is a sensitive parameter in the laser resonator configuration. The permissible angle of rotation, a function of the laser beam diameter, should be well within the diffraction limit of the active portion of the laser mirrors. The beamwidth relationship is given by

$$\theta = 1.22\frac{\lambda}{D}$$

where θ = beamwidth, in radians

λ = wavelength

D = (circular) beam diameter

Using the above as a criterion, the transmitter 6 mm diameter beam gives:

$$\theta = 1.22 \times \frac{10.6\times10^{-6}}{6\times10^{3}} = 2.16\times10^{-3} \text{ radians.}$$

If we allow a laser mirror rotation of $\theta/10$, we have

$$\theta_{\varepsilon} = 2.16\times10^{4} \text{ radians} \simeq 45 \text{ arcseconds.}$$

The mechanical tolerances necessary to limit the twist angle to 2.16×10^{-4} radians is computed below:

Assume that the moving element of the magnetic transducer is a beam supported on springs 2.5 cm apart (see Figure C-3). An angular error of 2.16×10^{-4} radian means, therefore, a relative motion at the two end points of

$$\Delta Z = 2.16\times10^{-4}\times2.5\times10^{-2} = 5.4\times10^{-6} \text{ meter.}$$

Since the twist angle is developed by a worst case mirror motion of 5.3×10^{-6} meters (i.e., a half wavelength at λ = 10.6 μm), we might reasonably assume that one corner of the element moves too much and the other too little, in equal amounts. Thus

$$(5.3+2.7)\times10^{-6} = 8.0\times10^{-6} \text{ meters} = \Delta Z \text{ maximum}$$

$$(5.3+2.7)\times10^{-6} = 2.6\times10^{-6} \text{ meters} = \Delta Z \text{ minimum}$$

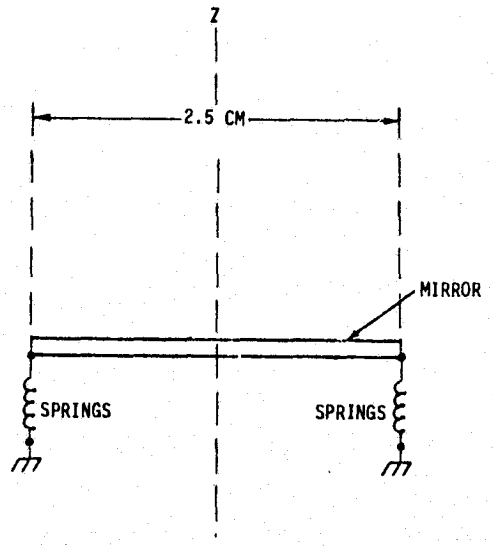

Figure C-3. Transducer Mechanical Schematic Diagram

implying a permissible ±50% tolerance on the spring rate* of the suspension.

With reasonable care a ±10% tolerance on the spring rate should be achieved, or five times better than the estimated requirements.

The above calculations assume that the magnetic force is uniformly applied to the moving element of the transducer. Since it is believed that the springs can be made more accurately than required, the design allows for torques corresponding to non-uniform magnetic forces (±40%) applied at the ends of the 2.5 cm moment arm.

---

*Spring rate is the force change (ΔF) per unit deflection (ΔZ)

C.5.4 Magnetic Effects

About 2/3 of the magnetic force will be concentrated at the center of the transducer in an area 0.75 cm in diameter. The magnetic field is largely governed by the air gap rather than the magnetic homogeneity of the materials. The materials will have a permeability greater than 1000. Since the reluctance of the air gap (with a uniform permeability of one) so far exceeds the reluctance of the magnetic materials, the material inhomogenities (typically ±20%) will be negligible in effect.

While nonuniformities in the air gap can have an effect, they can be controlled by careful machining and assembly of the transducer. The air gap will be about 0.25 mm. The machining tolerances will be within 0.01 mm over the center pole piece where most of the force is generated. This would give a 4% nonuniformity of the flux density and an 8% force unbalance over the 0.75 cm center pole area. Since the unbalance is distributed over the circular area of the pole rather than concentrated at the edges of a 0.8 cm moment arm, the net effect will be roughly equivalent to a 2% force unbalance applied at the ends of a 1.8 cm moment arm.

About 1/3 of the magnetic force is generated around the outer edge of the magnetic circuit. Because of moment arm effects when the moving element is not parallel to the pole faces of the magnet, the unbalance is magnified by 2.25 (ratio of outer to inner diameters). Therefore, a 0.01 mm tilt in the center pole is 0.0225 mm at the edges. This would give about an 18% force unbalance with the gradient distributed around the edge. However, since the unbalance acts at about 3/4 of the distance to the edge, it is equivalent to about 5% applied to a 1.8 cm moment arm.

The sum of the center and edge magnetic effects will be less than a 10% force unbalance applied on a 2.5 cm moment arm.

In conclusion, the mechanical and magnetic force unbalances are well within allowable limits. Figure C-4 illustrates the proposed transducer assembly.

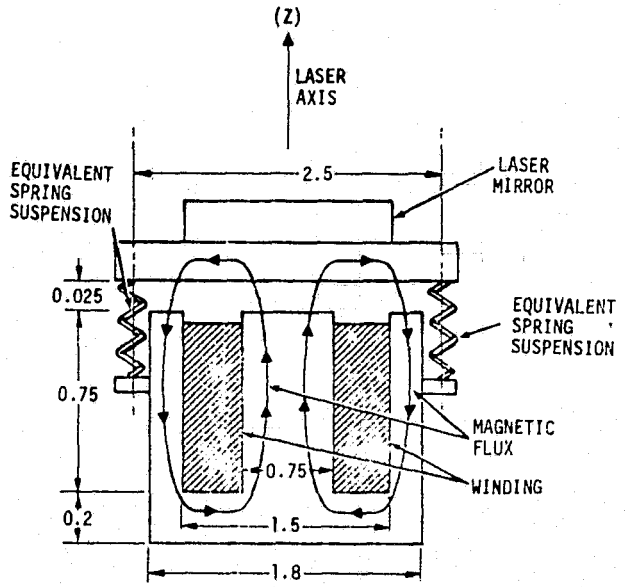

Figure C-4. Magnetic Laser Mirror Transducer

C.5.5 Spring Material Considerations

For the NASA laser sensor application, the following spring material requirements were considered:

a. Good elastic stability

b. High tensile strength (good spring material)

c. Non-magnetic

d. Good workability

e. Low temperature and controllable heat treatment, without furnace deterioration

f. Availability in desired thickness and widths.

Considering these requirements Beryllium Copper (BeCu) is the recommended material because:

a. Good elastic stability is achieved when heat treat time and temperature are applied to carry the tensility slightly beyond the crest of the tensile strength curves. BeCu has been heat treated in this way to produce pendulum accelerometer springs having good elastic stability and has been used in the ASB-1 bombing system.

b. A tensile strength of 165,000 - 175,000 psi can be achieved after heat treat.

c. BeCu is non-magnetic.

d. BeCu is readily workable in either the solution annealed condition or one-quarter hard condition.

e. Heat treatment is performed at temperatures less than 650°F. The material may be clamped between flat pieces of steel during the oven treatment. With the use of a non-oxidizing atmosphere during heat treatment, no scale and little or no stain develops.

f. A number of suppliers can furnish strip or plate stock 0.01 to 0.5 cm thick and 10 to 20 cm wide.

Several of the BeCu alloys have been designed to exhibit a low mechanical hysteresis for precision gyro applications. The maximum hysteresis for these materials is 0.0025%. Therefore, for a deflection of 5.3 micrometers the maximum hysteresis is:

$$5.3 \times 10^{4} \times 2.5 \times 10^{-5} = 1.325 \text{Å},$$

well within the 35Å allowable hysteresis error.

APPENDIX E

COMPUTER MODELING OF THE DOUBLE CONTROL LOOP

The control loop was simulated by means of the Tymshare CSMP (Continuous System Modeling Program), as described in a reference manual published by TYMSHARE, INC., Palo Alto., Calif. (1972).

The block diagram of the model is shown in Figure E-1. The computer program, embodying the configuration of Figure E-1, and containing all the approriate parameters, is shown in Figure E-2. It is to be noted that for the sake of conveience, the time scale is to be multiplied by 10^{-4}; i.e., each time unit is 0.1 millisecond. Other parameters have been appropriately scaled.

When the above program was run, the outputs of modules 4 and 15 were plotted on Figure 7, curves A and B, respectively.

The CSMP program lends itself to the simulation of the double-loop control system with any combination of values of the loop parameters, and should therefore be a valuable tool in the design and analysis of a final system.

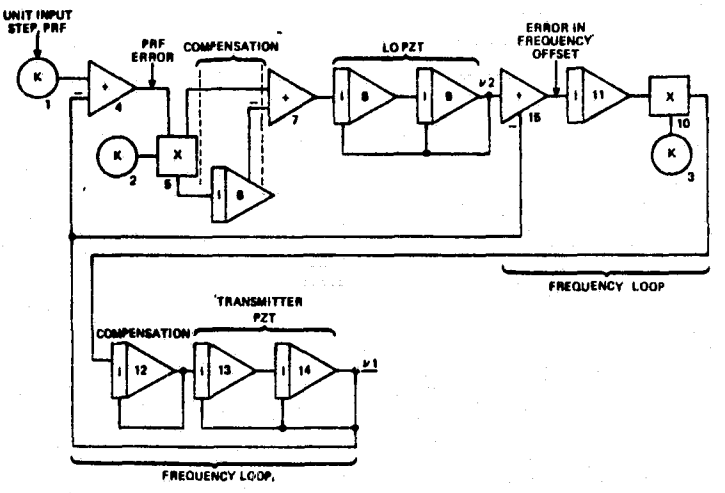

Figure E-1. CSMP Simulation Block Diagram

BLOCK	TYPE	E1	E2	E3	P1	P2	P3
1	K	0	0	0	1.000E 00		
2	K	0	0	0	1.300E-01		
3	K	0	0	0	1.860E-01		
4	+	1	-14	0			
5	X	4	2	0			
6	I	0	5	0	.000E 00	1.500E 00	
7	+	5	6	0			
8	I	0	7	9	.000E 00	2.470E 00	-2.470E 00
9	I	8	9	0	.000E 00	-5.236E-01	
10	X	11	3	0			
12	I	10	12	0	.000E 00	-6.283E-01	
13	I	0	12	14	.000E 00	2.470E 00	-2.470E 00
14	I	13	14	0	.000E 00	-5.236E-01	
15	+	9	-14	0			
11	I	15	0	0			

```
DT:  2.500E-01

OUTPUT
FROM:    .000E 00
BY:  1.000E 00
TO:  2.000E 01

RELERR:  1.000E-03

DTMIN:  2.500E-07

ALGORITHM: RK2
```

Figure E-2. CSMP Program Implementing Block Diagram of Figure E-1.